Growth faults above shale – seismic-scale outcrop analogues from the Makran foreland, SW Pakistan

Stefan Back[1] and Christopher K. Morley[2]

[1]EMR - Geological Institute, RWTH Aachen University, 52062 Aachen, Germany

[2]Department of Geological Sciences, Chiang Mai University, Chiang Mai 50200, Thailand

Email corresponding author: back@geol.rwth-aachen.de

Keywords: Growth fault, Pakistan, outcrop analogue, seismic-scale exposures, fault-damage zone, clinoforms

Abstract

The southern Makran fold-thrust belt, Pakistan, displays unique outcrop examples of well-exposed, kilometre-scale, listric growth faults that displace Miocene-age deltaic growth strata by several hundreds of metres to kilometers. The largest growth faults are counter-regional (landward-dipping), bounding major clastic depocentres exposed over areas > 1000 km^2. Stratal offset along these faults can exceed 1.5 km. Fault-zone thicknesses range between ca. 100 and 400 m, and average fault thickness-displacement ratios are around 1:10. High-resolution satellite data show in unprecedented detail the faults and the stratigraphic architecture of associated growth sequences, which comprise kilometre-scale progradational clinoforms, thick mudstone units and basinwards wedging sandstone-shale deposits. The true vertical thickness of the syn-kinematic record is, in places, up to 8 km, making the outcrop examples equivalent to major growth faulted successions known from seismic data of large deltas, and at least an order of magnitude larger than other outcrop examples. A comparison of the Makran outcrops with seismic-reflection examples offshore NW Borneo reveals distinct similarities in the gross depocentre geometries and internal architecture. The key control for growth faulting is interpreted to result from sedimentary loading, with rapid sedimentary progradation causing the development of rollover synclines by differential compaction and fluid expulsion, and counter-regional growth faults preferentially forming on the basinward side of these synclines. The data and interpretations presented can be used to assess the key parameters that contribute to the development of growth faults and growth successions above shale, reinforcing structural and stratigraphic observations from seismic interpretation and modelling studies in demonstrating their occurrence in exposure.

1. Introduction

In the broadest sense, the term growth fault applies to any fault that displays a syn-kinematic expansion of the hanging-wall section. However, the original meaning concerns basement-detached, gravity-driven, syn-sedimentary normal faults that typically die out into a detachment zone located within the sedimentary section (e.g. Bruce, 1973; Edwards, 1976; Lowell, 1985; Ellis and McClay, 1988; Mauduit and Brun, 1998, Hodgetts et al., 2001). This more restricted definition of the term growth fault is employed in this paper. The most common types of growth faults dip basinwards (Cloos, 1968; "regional faults" sensu Ocamb, 1961; "contemporaneous normal faults" sensu Hardin and Hardin, 1961), although major landward-dipping growth faults ("counter-regional faults" sensu Evamy et al., 1978) are also common. Both fault types form above ductile lithologies (commonly mudstones, overpressured shales or salt). The thicknesses of sedimentary units increase abruptly on the hanging walls of these faults, and a general progressive downward increase in displacement along much of the fault profile is common (Lowell, 1985).

The rapid accumulation of syn-kinematic deltaic sediment is thought to activate or re-activate growth faults by differential loading (e.g. Lundin, 1992; Damuth, 1994; Corredor et al., 2005; Back et al., 2006). However, once triggered, growth faulting influences depositional systems by forming fault-controlled depocentres (Thorsen, 1963; Bruce, 1973; McCulloh, 1988; Cartwright et al., 1998; Imber et al. 2003; Jackson and Larsen, 2009; Fazli Khani and Back, 2012; Fazli Khani and Back, 2015a). Consequently, both fault movement and the deposition of syn-kinematic sediment leads to internal structural-sedimentary feedback processes that ultimately contribute to a self-organized development of depositional systems.

Growth-faulted continental margins are known from many parts of the world from seismic-reflection data (Fig. 1), including: the US Gulf of Mexico (e.g. Lopez, 1990; Cartwright et al., 1998; Brown et al., 2004), NW Borneo (e.g. Sandal, 1996; Van Rensbergen and Morley, 2000; Hodgetts et al., 2001; Imber et al., 2003; Hiscott, 2003; Saller and Blake, 2003; Morley et al. 2003; Back et al., 2005; Back et al., 2008; Sapin et al., 2012), Namibia (DeVera et al., 2010; Butler and Paton, 2010), the Nile delta (e.g. Sestini, 1989; Beach and Trayner, 1991), and the Niger delta (e.g. Doust and Omatsola, 1989; Morley and Guerin, 1996; Rouby and Cobbold, 1996; Ajakaiye and Bally, 2002; Hooper et al., 2002; Pochat et al., 2004; Back et al., 2006; Fazli Khani and Back, 2012; Sapin et al., 2012). In these settings, the range of gravity-driven structures includes extensional syn-sedimentary faults of various shapes and scales, rollover anticlines with significant internal deformation, and mobile shale occurring layers, lenses, and diapirs. At the very basinward edge of the systems, contractional fold-and-thrust belts can develop. Yet, despite the widespread occurrence of growth faults and

their longstanding recognition as important petroleum traps (e.g. Jackson and Galloway, 1984; Doust and Omatsola, 1989), there are still open questions regarding their initiation, development and decay. For example, in deltas, rapid progradation of the sedimentary wedge, gravitational failure of the delta-front and gravitational gliding down delta slopes is commonly interpreted to control growth-fault initiation and development (Terzaghi, 1956; Bruce, 1973, Winker and Edwards, 1983; Garfunkel, 1984; Schlische, 1991; Gawthorpe et al., 1994). However, sand-loading on shale (Bruce, 1973), differential compaction and fluid escape (Carver, 1968; Bruce, 1973; Taylor et al., 2008; Van Rensbergen and Morley, 2000), footwall collapse above rising shale (Ocamb, 1961; Morley and Guerin, 1996), or the lateral and vertical linkage of faults (Cartwright et al., 1995; Rykkelid and Fossen, 2002; Walsh et al., 2003; Sapin et al., 2012; Tvedt et al., 2013; Rotevatn and Jackson, 2014) can also lead to the initiation of growth faults and contribute to their development through time. In numerical models of large prograding deltas, highly overpressured (90-95% lithostatic) shales are required for typical delta gravity tectonics to commence (Ings and Beaumont, 2010). In these models, the landward side of the extensional province develops regional faults, whereas counter-regional faults develop on the oceanward side.

The base of growth-faulted deltas or continental margin successions is usually deeply buried (> 5 km) and therefore difficult to image in seismic-reflection data. Consequently, the way in which deep-seated tectonic or stratigraphic features influence the development of younger overburden faults remain underexplored. Outcrops can provide further insights into the basal parts of deltas, but the enormous scale of growth-faulted successions makes them difficult to identify on usually restricted, in most cases tectonically overprinted outcrops. There are only few examples of well-exposed, outcropping growth faults, such as those exposed in Svalbard (Presthol and Walderhaug, 2000; Osmunsen et al., 2014), Utah (Bhattacharya and Davies, 2001; Fielding, 2015), the East Kentucky Coalfield, (Lewis et al., 2000), Ireland (Martinsen, 1989; Wignall and Best, 2004), Italy (Zecchin et al., 2004; 2006), France (Bouroullec et al., 2004), Chile (Shultz and Hubbard, 2005), Ischigualasto Provincial Park, Argentina (Albrecht, 2005) and onshore Borneo (e.g. Burhanudinnur and Morley, 1997; Morley et al., 2003; Back et al., 2005; van der Zee and Urai, 2005). However, these outcrop examples in tens to a few hundreds of meters scale are substantially smaller than the large, kilometre-scale growth faults imaged in seismic data of large deltaic provinces. Additionally, most of these exposures exhibit growth faults dipping basinward in the direction of sedimentary progradation, and only few counter-regional growth faults have been described (e.g. Bhattacharya and Davies, 2001; Shultz and Hubbard, 2005).

This study describes regional and counter-regional, kilometre-scale growth faults that offset associated growth strata by several hundreds of metres to kilometres. The faults are exposed in folded and rotated Miocene to Pliocene deltaic units of the Talar Formation in the foreland of the Makran fold and thrust belt, coastal onshore SW Pakistan (Fig. 2). The syn-sedimentary faults are imaged on medium-resolution Landsat ETM+ (15 m resolution) and high-resolution SPOT (2.5 m resolution) satellite data, permitting remote sensing-based geological analyses over hundreds of square kilometres with a resolution down to a few metres. Coupling of the satellite data with published sedimentological and stratigraphic data allows to differentiate between the tectonic signatures resulting from early syn-sedimentary faulting and post-sedimentary folding, supporting analyses of the original architecture of syn-sedimentary faults and syn-kinematic deposits prior to folding and exhumation. This analysis is finally compared to seismic subsurface growth-fault examples from offshore northwest Borneo and Nigeria.

2. Geological framework

The Pakistan part of the Makran coast is approximately 500 km long and extends from the Dasht River between Chabahar and Gwadar to the Sonmiani Bay northwest of Karachi (Fig. 2). The Cenozoic Makran fold and thrust belt formed during subduction of the Arabian plate below the Eurasian plate (Harms et al., 1984). Sediments within the fold and thrust belt are largely recycled erosional products of the India–Eurasia collision belt (Fruehn et al., 1997). Subduction probably started in the Paleocene (Platt et al., 1988), and accretion associated with thrusting and folding started in the Eocene (Byrne et al., 1992). The Oligocene is characterized by deposition of thick clastic sequences in a deepwater basin between SW Pakistan and SE Iran (Fruehn et al., 1997). The modern Makran accretionary prism initiated in the Late Miocene (Platt et al., 1985, 1988). The accretionary prism not only grew seaward by accretion of trench-fill sediments, but also by progradation of the slope, shelf and coastal plain (Grando and McClay, 2007). Accretion caused successive uplift of its landward portion above sea level, and subsequent erosion and re-sedimentation provided new material for continued accretion (Harms et al., 1984). During Miocene and Pliocene times, a major east-west oriented palaeo-delta (southwestern continuation of the Katawaz system of Quayyum et al., 1996; Carter et al., 2010) accumulated up to 10 km of sediment, occupying a large part of the present-day Makran region (e.g. CPCP, 1958; Hunting Survey Corporation, 1961; Ahmed, 1969; McCall and Kidd, 1982; Bannert et al., 1992; Figs. 2 and 3). Contractional deformation, uplift and exhumation of the palaeo-delta occurred in late Pliocene to recent times (Page et al., 1979; Snead, 1993). Since the Middle Pleistocene, the coastal part of the Makran has experienced significant uplift (1.5 mm/yr; White, 1983), associated with a pronounced seaward migration of the shoreline.

Today, the coastal areas of the Makran fold and thrust belt expose spectacular folds, faults, and intensively folded and faulted strata (Fig. 3). Structural and stratigraphic features of the Katawaz palaeo-delta have been rotated and exposed in map view, providing a multitude of natural cross-sections, some of 100's of kilometres extent. In the arid environment that characterises this region, satellite images reveal large-scale geological features such as major east-west trending progradational clinoforms, syn-sedimentary down-to-basin (regional) growth faults, kilometre-scale landward-dipping (counter-regional) growth faults, and internally deformed rollover anticlines. It is these features that form the focus of this study.

The geological map in Figure 3A and the stratigraphic column in Figure 4 shows a subdivision of the Neogene to Recent sedimentary succession of the Makran foreland into four major lithostratigraphic units: 1) the Panjgur Formation (ca. Oligocene-Middle Miocene), 2) the Parkini Formation (ca. Middle to Late Miocene), 3) the Talar Formation (ca. Late Miocene to Pliocene), and 4) the Chatti, Ormara and Jiwani formations (ca. Pliocene-Pleistocene). In various regional publications, the Parkini, Talar and Chatti formations, or parts of these, are combined as the Hinglaj or Makran groups (see Vredenburg, 1909; Ahmed, 1996; Cheema et al., 1977; Raza et al., 1990; Bannert et al., 1992; Snead, 1993; Bender and Raza, 1995; Delisle et al., 2002; Ellouz-Zimmermann et al., 2007). The Panjgur Formation, which occurs at the base of the succession, consists of mudstones intercalated with calcareous and micaceous, medium- to fine-grained sandstones (Ahmed, 1996; Critelli et al., 1990). Ellouz-Zimmermann et al. (2007) report abundant channels with mud-clasts at the base, current ripples, flute cast at the base of individual sandstone beds and Zoophycus-tracks, indicating a deepwater depositional setting (cf. Harms et al., 1984). The succession is either Oligocene to Early Miocene (CPCP, 1958; Ahmed, 1969) or Middle Miocene in age (NN5 to NN6, Ellouz-Zimmermann et al., 2007; see Fig. 4). Locally unconformably overlying this succession is the Parkini Formation, which is a calcareous mudstone unit interbedded with thin siltstones (Ahmed, 1969; Delisle et al., 2002) and occasional sandstone layers. These coarser clastics are generally a few centimetres thick, with abundant ripple marks (Ahmed, 1969). The coarser-grained intercalations increase in frequency upward towards the transitional contact with the overlying sandstones of the Talar Formation (Ahmed, 1969). Ellouz-Zimmermann et al. (2007) state that the Parkini Formation is generally rich in nanofossils of Zones NN9 to NN11 (Late Miocene), and interpret a generally shallowing-upward depositional trend for the succession (upper slope to outer shelf sedimentary environment). The partly time-equivalent Talar Formation (Fig. 4), on which this study mainly focuses, is dominated by medium- to coarse-grained sandstones, interbedded with shales

and mudstones (Ahmed, 1969). Individual sandstone beds are up to a few meters thick and are commonly characterized by cross-bedding, ripples marks and ichnofossils (Hunting Survey Corporation, 1961). In comparison to the underlying Parkini Formation mudstones, the Talar Formation sandstones seem relatively resistant to weathering, and the most sandstone-prone parts of this unit thus form the highest ranges in the study area. Ellouz-Zimmermann et al. (2007) report that the Talar Formation is rich in reworked species of Cretaceous to Upper Miocene ages, with rare autochthonous fossils. Critelli et al. (1990) assume a Late Miocene to Pliocene age for the Talar Formation (Fig. 4). At the top of the Neogene succession, the Talar Formation is overlain by the Pliocene (Ahmed, 1969; Critelli et al., 1990) to Lower Pleistocene (Ellouz-Zimmermann et al., 2007) Chatti Formation, which is a mudstone-dominated unit containing thin, interbedded siltstone layers and fine-grained sandstones. In places, thin, argillaceous and fossiliferous limestone beds are present (Hunting Survey Corporation, 1961; Ahmed, 1969). Within this unit, calcareous nanofossils are common, indicating a middle-outer shelf depositional environment (Ellouz-Zimmermann et al., 2007). The youngest deposits of the study area are shales, sandstones and conglomerates of the Ormara Formation and the coastal units of the Jiwani Formation (Fig. 3A), comprising limestones, conglomerates and sandstones (Ahmed, 1969).

3. Data and methods

The satellite data used in this study comprised 15 m resolution Landsat ETM+ panchromatic data and 2.5 m resolution SPOT 5 monochromatic images. As a standard procedure, the satellite images were overlain on ASTER digital elevation models (DEM) with a 30 m lateral resolution and a vertical accuracy (root-mean-squared-error) between 10 and 25 m (Tachikawa et al., 2011). Because the study area is composed of weathering-resistant sandstones alternating with highly weathered mudstones, the surface topography strongly resembles – at different scales - the general lithological trend. The combined analysis of DEM and high-resolution satellite data reveals many geomorphological elements related to surface lithology and lithological change, providing at ubiquitous locations links between topography, stratigraphy and tectonic elements. All remote-sensing-based interpretations were compared with the geological map of West Pakistan (CPCP, 1958) and the results of field studies (e.g. Vredenburg, 1909; Ahmed, 1969; Cheema et al., 1977; Raza et al., 1990; Critelli et al., 1990; Snead, 1993; Bender and Raza, 1995; Delisle et al., 2002; Ellouz-Zimmermann et al., 2007). At many sites, these studies permitted ground-truthing of satellite-based lithology predictions, tectonic interpretations and stratigraphic analyses, as well as providing local chronostratigraphic information (Fig. 3A). Estimates of the true stratigraphic thickness provided for all target locations was based on integrating dip data from aerial and surface surveying (CPCP, 1958; Hunting Survey Corporation, 1961), geological mapping

(Ahmed, 1969), ASTER DEM elevation and dip-measurements of large exposures, and qualitative stratigraphic interpretations based on the SPOT and Landsat ETM+ satellite data. Conversions of SPOT satellite data into pseudo-seismic images were finally applied at selected locations by using greyscale-coded surface-lithology estimates as relative impedance estimate (mudstone-dominated areas = light colors; sandstone-dominated areas = dark colors). Stratigraphically downward mudstone-sandstone contacts were defined by phase rotation as a relative impedance increase (trough, zero-phase, European polarity, indicated by red color). In turn, stratigraphically downward sandstone-mudstone contacts were defined as a relative impedance decrease (soft kick), corresponding to a seismic peak (zero-phase, European polarity, indicated by black color). The pseudo-reflectivity images were filtered to a synthetic frequency of 10 to 40 Hz to approximate the dominant frequency encountered in moderate-resolution industry-standard seismic-reflection data, deteriorating the initial 2.5-m-scale resolution of the input SPOT satellite image to a resolution of ca. 20 m.

4. Makran growth faults

The Landsat ETM+ satellite images of Figure 3B depict two areas in which major syn-sedimentary normal faults displace the westwards prograding deltaic units at the transition between Parkini Formation mudstones and the overlying sandstone-dominated Talar Formation. Figure 3B shows the western part of the Talar Syncline; folded strata north of the syncline axis dip towards the south and southeast, whereas bedding in the southern part of the syncline dips towards the northwest. Figure 3C shows the Buzi Range of the Hingol region. The Buzi Range forms the northern flank of the coastal Hinglay Syncline, with folded strata north of the syncline axis dipping in southeastern direction. The following paragraphs describe the geology exposed along the Buzi Range and in the Talar Syncline along the sediment transport direction from east to west.

4.1 Buzi Range

Figure 5 is a 200° counterclockwise (CCW) rotated and horizontally mirrored monochromatic SPOT satellite image of the central part of the Buzi Range blended with an ASTER digital elevation model (Fig. 5A), overlain by a fault and horizon interpretation (Fig. 5B), and the geological image interpretation (Fig. 5C). The rotation and mirroring places the satellite data into stratigraphic order (old deposits = bottom; young deposits = top), displaying the regional westward-oriented transport direction of the sedimentary system on the left side of the figure. All satellite data presented in the following are plotted the same way. The NW-SE trending sandstone-shale succession of the Buzi Range is exposed over a length of 20 km at elevations between 100 and 450 m; the outcrop-width perpendicular to the bedding is over 6 km, which equals approximately 4 km of true stratigraphic thickness (TST) after dip and

topography correction. The central part of the section is deformed by four large, listric, counter-regional (landward dipping) normal faults F1 to F4, each with an expanded sedimentary record (increase of layer thickness, in places additional layers; cf. Hodgetts et al., 2001) in their hanging walls. Stratal offset along the syn-sedimentary faults is generally highest at the lower fault tip below horizon 2 with 300 m (~150 m TST-corrected) at faults F2 and F4, 400 m (~200 m TST-corrected) at fault F1, and 1000 m (~500m TST-corrected) at fault F3. The upper tips of faults F1 and F2 terminate at horizon 5, whereas faults F3 and F4 terminate above horizon 8 (Figs. 5, 6). The four major counter-regional faults are accompanied by numerous secondary synthetic and antithetic faults with (TST-corrected) stratal offsets < 100 m. Some of these secondary faults form conjugate pairs in the hanging walls of the main growth faults F1 to F4. The chronostratigraphic chart of Figure 6 indicates that the location of the conjugate fault pairs shifts through time from the hanging-wall domain of the westernmost fault F1 against the main sediment-transport direction stratigraphically upwards into the hanging wall of faults F3 and F4. This shift seems associated with a general backstepping of counter-regional faulting towards the NW (Fig. 6) and subtle hanging-wall bending and collapse through time (Figs. 5, 6). Significant stratal bending at the level of horizon 8 in the hanging wall of fault F4 (Fig. 5) can be likely attributed to late-stage depositional loading of the sandstone-shale succession with massive, amalgamated sandstones. This loading affects only the hanging wall of faults F3 and F4; the older faults F1 and F2 remain unaffected by late-stage loading.

A multitude of small-scale synthetic and antithetic faults in the Buzi Range exposures west (basinwards) of fault F1 (Fig. 5B; also see Fig. 3C) displace the distal sandstone-shale succession between a few metres (offset detectability on the SPOT data ca. 5 m) up to ca. 60 m (TST-corrected). Neither depositional thickening within individual fault blocks nor preferential thickening across these faults was observed. Many of these fault are rooted in the shale and mudstone base of the Buzi Range succession (Figs. 5B, C), and differential compaction above this mud-rich substratum, possibly combined with fluid escape and hdro-fracturing can be interpreted to generate these structures. The base of the succession in the NE around horizon 1 is characterised by thick, internally deformed, partly chaotic sedimentary packages possibly deposited as slumps. These basal units are intersected by several eastward dipping, slightly listric structures, which may pass upward into faults F1, F3 and F4. Fault F2, however, is laterally offset by 400 m from an inferred deep-seated structure below (Figs. 5B, 5C).

4.2 Northern Talar Syncline

Figure 7 is a rotated (200° CCW) and horizontally mirrored monochromatic SPOT satellite image of the northwestern part of the Talar Syncline blended with an ASTER digital elevation model (Fig. 7A), overlain by a fault and horizon interpretation (Fig. 7B), and the geological image interpretation (Fig. 7C). The WSW-trending sandstone-shale succession is imaged along a > 60 km long section that lies at elevations between 50 and 800m. The oldest rocks at the base of the succession are mudstones of the Parkini Formation located in the north (base of figure), the youngest sedimentary units are mudstones of the Chatti Formation in the south (top of figure). The outcrop-width of the Talar Formation inbetween is – perpendicular to bedding – more than 14 km in the western part of the section, which equals > 8 km of true stratigraphic thickness (TST) after dip and topography correction. In the eastern, proximal part of the succession, the Talar Formation is exposed over ca. 7.5 km, which equals ca. 4 km of true stratigraphic thickness (TST). The Talar Formation thus forms a major westwards-thickening sedimentary wedge that terminates at the Dasht river in the vicinity of unstructured, massive Parkini Formation mudstones (Fig. 7B). Bedding dips within the Talar Formation are generally to the south, ranging between 60° at the basal contact to the Parkini Formation near horizon 1 to 5° at the transition to the Chatti Formation near horizon 10 (Fig. 7C). The base of the Talar Formation is characterized by kilometre-scale, sandstone-rich clinoforms that prograde from the east to the west and shale out in a major depocenter. Up section, sandstone-dominated units alternate with shale intervals of up to a few hundreds of meters thickness. The coarsest sediments characterise the middle part of the Talar succession, with massive, amalgamated sandstone units of over 1000 m thickness associated with depositional packages showing a maximum of westward progradation. In the proximal eastern part of the system, these units form a mountain range up to 950 m high. The youngest part of the Talar Formation is characterized by a pronounced retrogradation of the sedimentary system (Figs. 7A, B) and a conformable transition into the overlying Chatti Formation mudstones.

The sharp contact between the Talar Formation sedimentary wedge and the Parkini Formation in the vicinity of the Dasht river valley is interpreted to occur due to the presence of a kilometre-scale counter-regional growth fault accommodating the > 8 km (TST) expanded sedimentary record in the western depocentre. This fault displaces the massive sandstone units of the middle Talar Formation by 250 m near its upper termination. Stratal offset in the lower part of the fault is unclear due to the lack of a correlateable Talar Formation record on the footwall. At its very top, this major counter-regional fault is superseded by a younger, basinward-dipping normal fault. The few minor synthetic and antithetic faults that displace the hanging-wall succession of this major structure are probably

related to stratal bending, but successive conjugate collapse systems as observed in the Buzi Range example (Fig. 5) are lacking in the northern Talar Syncline.

4.3 Southern Talar Syncline

Figure 8 is a 20° clockwise (CW) rotated monochromatic SPOT satellite image of the southwestern Talar Syncline (Fig. 3) blended with an ASTER digital elevation model (Fig. 8A), overlain by a fault and horizon interpretation (Fig. 8B), an overview geological interpretation (Fig. 8C) and a detailed structural interpretation of the fault zone between faults X1 and X2 (Fig. 8D). North is at the top of the figure, south at the base. The WSW-trending sandstone-shale succession of the Talar Formation is imaged along a section ca. 30 km long, exposed at elevations between 50 and 300 m. The outcrop-width perpendicular to the bedding is in places 10 km, which equals to ca. 3.5 km of true stratigraphic thickness (TST) after dip and topography correction. True stratigraphic thickness between horizons 4 and 10 is in the west of the section approximately 3 km, in the central part around 2.3 km, recording a moderate thickening of the Talar Formation sandstones (particularly those above horizon 8) in westerly direction in the order of a few hundreds of metres. Bedding dips are generally to the north, ranging between 20° at the base of the succession to horizontal in the syncline centre (Fig. 8C). The sandstone-shale interbeds of the Talar Formation bend westwards into a complex array of normal faults. In comparison to the northern part of the Talar Syncline, the sediments exposed in the south are less resistant to erosion and form generally low hills. The youngest part of the succession shows an increase in shale content and a conformable transition into the overlying Chatti Formation mudstones.

The main fault zone towards the top of the section comprises two main faults (faults X1 and X2; Figs. 8C, D) that are about 2 km apart. Fault X1 separates a shale prone Parkini Formation section (PK on Fig. 8C) from a relatively condensed sandstone-shale hanging-wall succession, while fault X2 lies within the sandstone-shale succession and has a comparably expanded section on its eastern (hanging-wall) side. The lower (L) and lower-middle (M) units (horizons 4 to 7) display similar stratal offsets between fault X1 and the hanging wall of fault X2. However, for the upper part of unit M the horizon displacement is focused on fault X2, while in the lower part of unit M stratal offset seems distributed on more faults. In unit L there are numerous connected and isolated faults in the 4 km zone between faults X1 and X2. In the western splay (X2b) of fault X2, large-scale smear-zones in sand-shale sequences can be inferred that are associated with an apparent stratal offset of about 900 m (Fig. 8D).

The eastern part of the southern Talar Syncline shows a pronounced bending of the Talar Formation sandstone-shale interbeds from southwestern strike to an ESE-WNW strike (Fig.

3). Figure 9A is a rotated (15° CW) monochromatic SPOT satellite image of the southeastern Talar Syncline converted into true stratigraphic thickness (TST), imaging numerous, dominantly normal faults displacing the zone of maximum stratal bending (sandstone- and siltstone-dominated lithology = dark colors; mudstone-dominated lithology = light colors). Figure 9B shows a fault and horizon interpretation, documenting horizon offsets by synthetic and antithetic normal faults between a few metres up to 160 m. In places, subtle across-fault thickening of the hanging-wall strata up to a few tens of metres can be observed, indicating that extensional faulting was syn-depositional. The two graben systems in the centre of the image formed likely contemporaneously between the development of horizons 3 and 4 (Fig. 9B). The activity of the western system ceased at the time of development of horizon 4; the western bounding fault of the more proximal, eastern graben system was probably active beyond the development of horizon 6 (Fig. 9B). In addition to normal faulting, some reverse faulting affects the eastern part of the southern Talar Syncline, most clearly imaged between horizons 1 and 4 on the western side of Figure 9B. Other reverse faults associated with stratal offsets of a few tens of metres can be observed in the western continuation of horizons 1 to 4 on the Landsat ETM+ data of the basal Talar Formation sandstones shown in Figure 3B. These faults likely formed post-depositionally due to Pliocene to Recent compression, and a reverse overprint can be expected to have contributed to some extent to the variable fault dips and stratal offsets observed in Figure 9B.

Figure 9C is a conversion of the SPOT satellite image into pseudo-reflectivity data using the surface-lithology information as relative impedance estimate. The pseudo-reflectivity data is filtered to a synthetic frequency of 10 to 40 Hz (resolution of ca. 20 m). Figure 9D compares a medium-resolution seismic-reflection section (zero-phase; European polarity; frequency 5 to 60 HZ) and well data across a deltaic rollover with an extensionally faulted crest from the Niger Delta. The outcrop-seismic comparison of the Makran and Nigeria data suggests that conjugate faults present at the eastern end of the southern Talar Syncline (Fig. 9C) are rather atypical for conjugate faults typically seen on seismic reflection data, in that many of them steepen downwards. This geometry can be partly due to compressional structural overprint deforming original fault geometry; however, these faults are also reminiscent of the secondary convex-upwards listric faults generated in analogue experiments of major listric growth faults by McClay et al. (1991). These authors noted that such convex-upwards faults may not easily be interpreted on seismic reflection data. The observations made here thus may reinforce the results of analogue models in demonstrating their occurrence in nature.

5. Discussion

Both, the Buzi Range and the Talar Syncline are characterised by major syn-sedimentary faults that displace the kilometre-thick sandstone-shale units of the Talar Formation by several hundreds (Buzi Range; Figs. 5, 6) to a few thousands of metres (western Talar Syncline; Figs. 7, 8). These structures are clearly of a scale comparable to that of subsurface faults imaged in seismic-reflection data. The lateral continuity of the outcrop sections over several tens of kilometers enables a comparison of the structural and stratigraphic depocentre architecture of the Makran exposures with growth faults known from other field areas, as well as large-scale growth faults imaged in subsurface seismic-reflection data. With respect to outcrop data of other regions, the dip-perspective extent and stratal offset of the exposed fault zone illustrated in Figure 8 is large. For example, the Moab Fault in the Moab Valley near Arches National Park, Utah, is exposed over a strike length of about 45 km with a maximum displacement of about 960 m (Foxford et al., 1998). This fault zone is emphasised because the exposures are a favourite stop for academic and industry fieldtrips with an interest in fault-zone processes and products in sedimentary basins. The exposures yet reveal a predominantly strike-view of the fault, with only limited vertical sampling of the fault zone, but have become important localities for understanding fault seal, fault damage zones, and the impact of faulting on clastic reservoirs (e.g. Foxford et al., 1998; Eichhubl et al., 2009). The popularity of the Moab Fault highlights the comparative rarity of well-exposed large normal fault zones. The Gulf of Suez rift is another classic area for well-exposed normal faults (e.g. Jackson et al., 2006) that are seen predominately in strike-view, with a limited dip perspective. In contrast, the southern Talar Syncline exposes a major, complex fault zone in syn-kinematic sediments in (apparent) dip perspective over a distance of 12 km, in a region of almost 100% exposure. It presents therefore a possibly unique opportunity to view the architecture of a major growth fault from near surface to about 4 km depth. Unfortunately the key difference with the Moab Fault is accessibility.

The largest growth faults are today almost entirely known from seismic reflection data, which have limited resolution, particularly in more deeply buried parts of a basin. The properties of large fault zones (such as fault damage-zone characteristics, displacement-thickness relationships, shale smear-displacement relationships) are extrapolated from measurements at the lower size range from outcrop or core. Many fundamental fault-zone characteristics seem to be fractal over a wide range of scales (e.g. Walsh and Watterson, 1988; Cowie and Scholz, 1992; Dawers et al., 1993; Ouillon et al., 1995; Odling et al., 1999; Kim and Sanderson, 2005; Shipton, 2006; Manzocchi et al., 2008). However, large faults can differ from smaller faults in several significant ways: 1) they are active over a broader temperature and pressure range; 2) as a consequence of 1) the basal fault zone may tap into deeper, hotter fluids than smaller faults, and the basal detachment (if one is present) will deform

under different conditions than much of the fault zone; 3) the duration of activity is likely longer; 4) large-displacement faults can affect other large-scale processes (e.g. flow in shales, crustal isostatic responses, sedimentation processes); and 5) they have a higher potential for seismogenic activity. Hence it is important to be able to investigate large faults in outcrop to test the validity of the fractal assumptions, and how they may vary from smaller fault zones.

It is rare to get displacement-thickness data for very large fault zones (e.g. Shipton et al., 2006; Manzocchi et al., 2008), but the southern Talar Syncline major growth fault zone (Fig. 8) provides some estimates from measuring either: 1) the width of the zone where beds are smeared into the orientation of the fault zone, or 2) the gap between closest points in the hanging- and footwalls where beds exhibit typical strikes that are unaffected by faulting. These are estimates for the damage zone, not just the fault core, and are probably maximum estimates. Widths of the damage zone arounf fault X2 are on average around 100 m, in the best developed smeared zones widths are up to 200 m (Fig. 8D). Very locally where splaying faults join the fault zone, widths increase to a maximum of about 400 m. Displacement estimates are difficult to make due to the oblique section; however, the measured stratal offset is in the order of 500-1500 m for these zones. Hence average thickness:offset ratios are around 1:10, but very locally can be reduced to 1:3 to 1:4. These estimates are in line with thickness:displacement ratios determined from multiple fault data sets (Shipton et al., 2006; Manzocchi et al., 2008).

The complexity of faulting within the South Talar growth fault zone is reminiscent of many of the features of smaller-scale growth fault zones (e.g. Burhanudinnur and Morley, 1997; van der Zee and Urai, 2005). However, the interaction of the section with the sedimentary section is different. The lowest units were likely deposited when deformation was widely distributed on numerous faults, and passing up-section deformation became more focussed on fault X2 (Fig. 8C, D). In smaller faults such a change in geometry might be regarded as a consequence of random fault splay or fault linkage events, or some influence of mechanical stratigraphy. For the South Talar growth fault the change could be also a consequence of the early syn-kinematic depocentre geometry, with deformation evolving from distributed to focussed with time. Displacement in the lower unit seems to have been accommodated by more ductile deformation (folding) as well as faulting, changing to dominant brittle deformation in the middle and upper units.

No examples of how major growth faults behave once they pass into the shale detachment zone are known from outcrop. Only relatively small detachments have been described (e.g.

Albrecht, 2005; Osmundsen et al., 2014). Consequently the behaviour of shales associated with growth fault detachments at depths of 3-4 km is undocumented, and it remains uncertain whether shales flow and form diapirs, or just form narrow, weak, overpressured fault zones with limited flow (see discussions in Day-Stirrat et al., 2010; Morley et al., 2011). Adjacent to the main growth faults), in the shale-prone section well-bedded units are present in places (Fig. 8 A, B). This observation at least indicates the shaley section is not simply a complexly folded ductile flow unit, and if ductile flow did occur it was confined to certain zones only, not the entire shale mass. There are geometries that suggest shale could have been squeezed into a broad bulge in the footwall of a counter-regional growth fault. But to resolve the problem further requires field observations.

For a regional outcrop to seismic comparison, Figure 10 shows a synoptic view of the rotated (200° CCW) and horizontally mirrored SPOT image of the northern Talar Syncline succession (Fig. 10A) and the major Plio-Pleistocene Perdana-Frigate depocentre offshore NW Borneo (Fig. 10B; Hesse et al., 2009, 2010). The Perdana-Frigate depocentre is bound in the west by the counterregional Perdana-Frigate fault, a syn-sedimentary normal fault with up to a few kilometres displacement (Van Rensbergen and Morley, 2000) that extends laterally over more than 50 km (Morley, 2007). The central part of the fault-bound Perdana-Frigate depocentre exhibits a kilometre-scale rollover anticline with a collapsed crest. A comparison with the Makran satellite data (Fig. 10A) reveals distinct similarities in the gross structural geometry and internal stratigraphic architecture of the fill of the offshore Borneo and onshore Pakistan depocentres. Prominent features on both datasets are, for example, the kilometer-scale, westwards-prograding clinoforms in the lower part of the basin fill that are superseded by basinwards wedging sediments, and the major syn-sedimentary faults on both landward and seaward sides of the basins, with the western, basinward-bounding counter-regional faults respectively intersected at the top by a younger, seaward-dipping normal fault. The lateral and vertical scale of the outcrop data remains, after dip correction, twice of that of the seismic example, which underlines the enormous scale and continuity of the Makran exposures.

The Makran SPOT data furthermore allows a detailed view into the outcrop stratigraphy (detectability of beds ~ 5 m), which can contribute to the understanding of sedimentary architecture imaged on lower resolution seismic-reflection data. Figure 11 is a close-up of the sandstone-shale units at the base of the northern Talar Syncline (Fig. 11A, B, C) compared to a flattened zoom-in of the basal clinoforms of the Perdana-Frigate depocenter (Fig. 11D). The westward-prograding clinoform succession of the Talar Syncline shows a pronounced basinward thinning, and, at the clinoform topsets, a shift from depositional aggradation to

downstepping with a continued seaward shift of the sedimentary system (Fig. 11A, B). Conversely, in the overlying stratigraphic intervals, clinoform geometries are lacking and all sedimentary units thicken basinwards into the western bounding fault (Fig. 10; also see succession tops on Figs 11A, B). A comparable scenario can be interpreted from the 2D seismic-reflection section of the Perdana-Frigate depocentre (Figs. 10B; 11D), where stacks of prograding clinoforms precede the formation of a basinward thickening, fault-controlled wedge in the hanging wall of the major western bounding fault. Limited seismic resolution and reflection continuity due to the intense faulting above, however, makes the detection and interpretation of reflection terminations within the Perdana clinoform succession difficult (Figs. 10B, 11D).

The outcrop-seismic comparison of the Makran and Borneo examples thus documents on regional scale the formation of a major pre-growth clinoform succession in both systems, succeeded by a kilometre-scale sequence of syn-kinematic growth strata. The onset of counter-regional faulting started latest with the deposition of the oldest growth strata, and, if driven by sedimentary loading, most likely in an interval marked by a change in the balance between sediment input and accommodation. The prograding clinoforms at the succession base indicate sediment-surplus conditions, retrogradation of the depositional system implies an accommodation surplus, and the final sedimentary wedging suggests an approximate balance between fault-controlled accommodation creation and sediment accumulation. The pronounced retrogradation of the Talar Formation sandstones above the basal clinoforms (Fig. 11A) could be interpreted to represent the onset of faulting rapidly creating accommodation that outpaced sediment accumulation. The distinct basinward thickening and divergence of all sedimentary units above (Figs. 10A, 11A) indicates major syn-kinematic sedimentation, which is comparable in the Perdana-Frigate depocenter offshore NW Borneo (Fig. 10B). Figure 12A is a schematic illustration of an entirely sedimentation-driven mechanism (cf. Ge et al., 1997; Jackson et al., 2015) that could control the initiation of counter-regional growth faults in front of prograding clinoforms, in which differential loading, compaction and possibly fluid expulsion create synclines on the clinoform bottomsets that potentially trap turbidite and slope sediments. Further preferential and rapid sediment accumulation in such a loading-induced depocenter could lead to fault initiation between the syncline fill and less compacted deposits basinward. The lower-tip termination of the main bounding faults within the stratigraphy in both, the Talar Syncline (Figs. 7, 10A) and Perdana-Frigate examples (Fig. 10B, 11D), the overall bowl-shape of the depocentres, and the lack of a connection of the master growth faults to older, deep-seated structures support this interpretation. While reactivation of old thrusts as normal faults is a viable explanation for

the development of some counter-regional faults (Sapin et al., 2012), we suggest that other mechanisms need to be considered as well (e.g. Fig. 12).

The structural and stratigraphic style of the Buzi Range succession (Fig. 5) differs from the Talar Syncline and Perdana-Frigate examples by lacking a general depocentre shape (Fig. 4C), an isolated master fault-system controlling sedimentation, and large-scale clinoforms. The counter-regional growth faults within this succession are much smaller than those of the Talar Syncline and NW Borneo in both, vertical extent and displacement, which is yet larger than that of the multitude of small, basinward faults that can be explained to have formed by differential compaction, possibly combined with fluid escape and hydrofracturing. Figure 5 shows the counter-regional faults F1 to F4 of the Buzi Range to have formed in an area underlain by internally deformed, possibly slumped, likely mudstone-rich lithology. In this case, compaction and dewatering of the waterlogged, undercompacted substratum by loading with Talar Formation sandstones could have provided extra accommodation filled with sedimentary units ultimately detaching along a landward dipping fault plane from their basinward stratal continuation (Fig. 12B). The interpretation of such an initiation of counter-regional faulting varies from the Talar Syncline and Perdana-Frigate case (Fig. 12A) in that solely the nature of the pre-existing substratum initially controls the generation of space, which, when filled, differentially compacts and reacts to further loading until finally reaching a stable compaction state (Fig. 12B). Pre-existing, potentially landward-dipping structural weaknesses in the substratum, such as potential slump toe-thrusts in the substratum of the Buzi Range succession, can likely contribute to the development of such smaller-scale counter-regional growth faults.

Irrespective of the mechanism of initiation, both the models presented above depend on the formation of an initial syncline that evolves into a persistent depocentre. Sedimentary loading further increases compaction and fluid loss in the syncline substratum, outpacing compaction in the surrounding areas. The high rate of loading-driven subsidence in the depocentre eventually causes stratigraphic rupture and growth faulting between the syncline fill and the less compacted, less subsiding basinward footwall strata (Fig. 12). The northern Talar Syncline, Buzi Range and Perdana-Frigate examples can be interpreted as an entirely loading-driven development of an initial syncline. However, this interpretation is not required if deeper-seated structures such as thrust faults or diapirs provide landward structural lows that are preferentially loaded (Fig. 13; also see Sapin et al., 2012). Such tectonically controlled depocenters will act in a similar way to their loading-initiated counterparts in compacting and subsiding more rapidly than their surroundings, and ultimately generate comparable fault and stratigraphic geometries. For the western part of the southern Talar

Syncline (Fig. 8), the possible presence of deep-seated, pre-existing thrust faults or shale movement/diapirism within the Parkini Shales cannot be excluded.

6. Conclusions

1. The southern foreland of the Makran fold-thrust belt, SW Pakistan, exposes major extensional growth faults that displace the kilometre-thick sandstone-shale units of the Miocene Talar Formation by several hundreds to a few thousands of metres. The synsedimentary structures are of a scale comparable to that of major subsurface growth faults imaged in seismic-reflection data.

2. High-resolution satellite data show in unprecedented detail the structural and stratigraphic architecture of growth faults and growth sequences, which can be considered as field analogues for buried systems imaged in low-resolution geophysical subsurface data. The southern Talar Syncline e.g. provides over kilometres estimates for the width of damage zone at growth faults ranging between ca. 100 and 400 m. Displacement estimates are difficult to make due to the obliquity of the satellite image with respect to structures and stratigraphy, but stratal offsets in the order of 500-1500 m for these zones seem reasonable. Hence average damage-zone thickness:offset ratios are probably around 1:10, but very locally can be as little as 1:3 to 1:4.

3. The southern Talar Syncline furthermore shows conjugate faults at its eastern end that are rather atypical for conjugate faults typically seen on seismic reflection data, in that many of them steepen downwards. These faults are reminiscent of secondary convex-upwards listric faults generated in analogue experiments of major listric growth faults.

4. The sedimentary succession of the northern Talar Syncline exhibits on a regional scale major prograding clinoforms in the lower part of the basin fill, succeeded by basinwards wedging growth strata. A similar association of large-scale pre-growth clinoforms followed by kilometre-scale synkinematic growth strata is imaged on seismic analogue data from offshore NW Borneo. The outcrop-seismic comparison of the Makran and Borneo examples suggests that sedimentation likely controlled the initiation of counter-regional growth faults in front of prograding clinoforms by differential loading, compaction and fluid expulsion that created synclines at the clinoform bottomsets; subsequent preferential sedimentation in these depocenters could have led to stratal rupture and fault initiation between the syncline fill and less compacted deposits basinward.

5. Counter-regional growth faults exposed in the Buzi Range differ from those of the Talar Syncline and NW Borneo in vertical extent and the amount of displacement. These smaller-scale structures are interpreted to have developed above slumped, mudstone-rich, potentially waterlogged and undercompacted lithologies. Compaction and dewatering of the substratum by sedimentary loading likely provided extra accommodation in the form of a bowl-shaped depocentre, with the depocentre fill detaching along a landward dipping fault plane from their basinward stratal continuation.

6. The geological interpretations of the Makran satellite data are uncorrected for topographic distortion and variable subsurface dips; the Makran outcrop sections are thus not directly comparable to true vertical geological cross-sections. The exposure of growth faults and growth stratigraphy along large, relatively simple folds nevertheless permits qualitative geological analyses over vast areas with a resolution down to a few metres. Regional 3D structural modelling and unfolding could be applied to restore rotated structures and stratigraphy back to their original position, which would enable quantitative satellite-based analogue analysis.

Acknowledgements

The authors thank the USGS for providing Landsat ETM+ data, NASA for providing ASTER-DEM data, and CNES for providing SPOT data under ISIS-grant 286. Seismic data offshore NW Borneo were kindly provided by the Federal Institute for Geosciences and Natural Resources (BGR) in the framework of projects Ba 2136/2-1, 2-3 and Fr 2119/1-1 funded by the Deutsche Forschungsgemeinschaft (DFG). Shell Petroleum Development Company of Nigeria (SPDC) is thanked for providing Nigeria seismic data. Seismic Micro-Technology (SMT) is gratefully acknowledged for providing the KingdomSuite+ under an Educational User License Agreement, Schlumberger is gratefully acknowledged for providing Petrel under an Academic User License Agreement, and Philipp Konerding is thanked for providing the software kogeo for bitmap to seismic conversion. We also thank J. Dreßel, H. Fazli Khani, D. Franke, T. Kampmann, C. Lentowitsch, J. Niederau and H. Schulz for their input in the research presented. This study is a contribution to project Ba 2136/4-1 funded by the Deutsche Forschungsgemeinschaft (DFG). We thank Christopher Jackson and an anonymous reviewer for constructive comments that helped improve the manuscript.

References

Ahmed, S.S., 1969. Tertiary Geology of Part of South Makran, Baluchistan, West Pakistan. AAPG Bulletin, 53, 1480-1499.

Ajakaiye, D.E. and Bally, A.W., 2002. Course Manual and Atlas of Structural Styles on Reflection Profiles from the Niger Delta: Continuing Education Course Note Series, 41, American Association of Petroleum Geologists, Tulsa, 106 p.

Albrecht, T.L., 2005. A Triassic syndepositional detachment system, Ischigualasto Provincial Park, Northwest Argentina. MSc. Thesis, Miami University, 56 p.

Armandita, C., Morley, C. and Rowell, P., 2015. Origin, structural geometry, and development of a giant coherent slide: The South Makassar Strait mass transport complex. Geosphere, 11, 376-403.

Back, S., Tioe, H.J., Thang, T.X. and Morley, C. K., 2005. Stratigraphic development of synkinematic deposits in a large growth-fault system, onshore Brunei Darussalam: Journal of Geological Society of London, 162, 243-258.

Back, S., Höcker, C., Brundiers, M. B. and Kukla, P.A., 2006. Three-dimensional-seismic coherency signature of Niger Delta growth faults: integrating sedimentology and tectonics: Basin Research, 18, 323–337.

Back, S., Strozyk, F., Kukla, P.A. and Lambiase, J.J., 2008. 3D restoration of original sedimentary geometries in deformed basin fill, onshore Brunei Darussalam, NW Borneo. Basin Research, 20, 99-117.

Balsamo, F., Storti, F., Piovano, B., Salvini, F., Cifelli, F. and Lima, C. 2008. Time dependent structural architecture of subsidiary fracturing and stress pattern in the tip region of an extensional growth fault system, Tarquinia basin, Italy. Tectonophysics, 454, 54–69.

Bannert, D., Cheema, A., Ahmed, A. and Schäfer, U., 1992. The structural development of the Western Fold Belt, Pakistan. Geologisches Jahrbuch, 80, 60 p.

Baudon, C. and Cartwright, J., 2008. Early stage evolution of growth faults: 3D seismic insights from the Levant Basin, Eastern Mediterranean. Journal of Structural Geology, 30, 888–898.

Beach, A. and Trayner, P., 1991. The geometry of normal faults in a sector of the offshore Nile Delta, Egypt. In Roberts, A.M., Yielding, G. and Freeman, B., The Geometry of Normal Faults: London, Special Publication of the Geological Society of London, 56, 173-182.

Bega, Z. and Ionescu, G., 2009. Neogene structural styles of the NW Black Sea region, offshore Romania. The Leading Edge, 28, 1082-1089.

Bender, F. K. and Raza, H. A., 1995. Geology of Pakistan. Gebrüder Borntraeger, Berlin, 414 p.

Bhattacharya, J., and Davies, R.K., 2001. Growth faults at the prodelta to delta front transition, Cretaceous Ferron Sandstone, Utah. Marine and Petroleum Geology, 18, 525-534.

Bouroullec, R., Cartwright, J. A., Johnson, H. D., Lansigu, C., Quemener, J.-M. and Savanier, D., 2004. Syndepositional faulting in the Gres d'Annot Formation, SE France; high-resolution kinematic analysis and stratigraphic response to growth faulting. In Joseph, P. and Lomas, S. A. (eds.), Deep-water sedimentation in the Alpine Basin of SE France; new perspectives on the Gres d'Annot and related systems. Geological Society Special Publications, 221, 241-265.

Brown, L.F.Jr., Loucks, R.G., Trevino, R. H. and Hammes, U., 2004. Understanding growth-faulted, intraslope subbasins by applying sequence-stratigraphic principles: examples from the south Texas Oligocene Frio Formation: American Association of Petroleum Geologists Bulletin, 88, 1501-1522.

Bruce, C., 1973. Shale tectonics, Texas coastal area growth faults, in Bally, A. W., ed., Seismic expression of structural styles: American Association of Petroleum Geologists Studies in Geology, 15, 878-886.

Burhannudinnur, M. and Morley, C.K., 1997. Anatomy of growth faults in poorly lithified sandstones and shales: implications for reservoir studies and seismic interpretation: Part 1 Outcrop Study. Petroleum Geoscience, 3, 211-224.

Butler R.W.H. and Paton, D.A., 2010. Evaluating lateral compaction in deepwater fold and thrust belts: How much are we missing from "nature's sandbox"?, GSA Today, 20, 4-10.

Byrne, D.E., Sykes, L.R. and Davis, D.M., 1992. Great thrust earthquakes and aseismic slip along the plate boundary of the Makran subduction zone. Journal of Geophysical Research, 97, B1, 449-478.

Carver, R. E., 1968. Differential compaction as a cause of regional contemporaneous faults. AAPG Bulletin, 52, 414–419.

Carter, A., Najman, Y., Bahroudi, A., Bown, P., Garzanti, E. and Lawrence, R.D., 2010. Locating earliest records of orogenesis in western Himalaya: Evidence from Paleogene sediments in the Iranian Makran region and Pakistan Katawaz basin. Geology, 38, 807–810.

Cartwright, J.A., Bouroullec, R., James, D. and Johnson, H.D., 1998. Polycyclic motion history of Gulf Coast Growth Faults from high resolution kinematic analysis: Geology, 26, 819-822.

Cartwright, J.A., Trudgill, B.D., Mansfield, C.S., 1995. Fault growth by segment linkage: An explanation for scatter in maximum displacement an trace length data from the Canyonlands Grabens of SE Utah. Journal of Structural Geology, 17, 1319-1326.

Chapman, T.J. and Meneilly, A.W., 1991. The displacement patterns associated with a reverse-reactivated, normal growth fault. In: Roberts, A. M., Yielding, G. and Freeman, B. (eds.), The Geometry of Normal Faults, Geological Society Special Publication, 56, 183-191.

Cheema M.R., Raza S.M. and Ahmad, H., 1977. Cenozoic: in Shah, S.M.I. (ed.), Stratigraphy of Pakistan: Geol. Sur Pakistan, Quetta, Memoir, 12, 56-98.

Chimney, P. and Kluth, C., 2002. Evidence for low-angle, subhorizontal hanging faults in rotated fault blocks, Cabinda, offshore Angola. The Leading Edge, 21, 1084-1090.

Chisholm, J.I. and Waters, C.N., 2012. Syn-sedimentary deformation of the Ashover Grit (Pennsylvanian, Namurian, Marsdenian Substage) deltaic succession around Wirksworth, Derbyshire, UK. Proceedings of the Yorkshire Geological Society, 59, 25-36.

Choudhuri, M., Sinha, S.T. and Sinha, N. 2008. Relationship between localization of shale bulges/toe thrusts and basement structures. 7th Biennial International Conference and Exposition on Petroleum Geophysics, Hyderabad. Extended Abstract P–399.

Cloos, E., 1968. Experimental analysis of Gulf Coast fracture patterns. AAPG Bulletin 52, 420-444.

Cobbold, P.R., Mourges, R. and Boyd, K., 2004. Mechanism of thin-skinned detachment in the Amazon Fan: assessing the importance of fluid overpressure and hydrocarbon generation. Marine and Petroleum Geology, 21, 1013-1025.

Corredor, F., Shaw, J. H. and Bilotti, F., 2005, Structural styles in the deep-water fold and thrust belts of the Niger Delta: American Association of Petroleum Geologists Bulletin, 89, 753–780

Cowie, P.A. and Scholz, C.H., 1992. Displacement-length scaling relationship for faults: Data synthesis and discussion. Journal of Structural Geology, 14, 1149-1156.

Crame, J. A., 1984. Neogene and Quaternary Mollusca from the Makran Coast, Pakistan. In: Haq, B. U. and Milliman, J. D. (eds.), Marine Geology and Oceanography of Arabian Sea and Coastal Pakistan. VNRC, New York, 45-61.

Critelli, S., de Rosa, R. and Platt, J.P., 1990. Sandstone detrital modes in the Makran accretionary wedge, southwest Pakistan: implications for tectonic setting and long-distance turbidite transportation. Sedimentary Geology, 68, 241-260.

CPCP, 1958. Reconnaissance Geology of Part of West Pakistan, Colombo Plan Cooperative Project, Geological Maps No. 4 and 5, Pasni/Ormara.

Cummings, D.I. and Arnott, R.W.C., 2005. Growth-faulted shelf-margin deltas: a new (but old) play type, offshore Nova Scotia. Bulletin of Canadian Petroleum Geology, 53, 3, 211-236.

Curtis, D., 1986. Comparative Tertiary petroleum geology of the Gulf Coast, Niger, and Beaufort-Mackenzie delta areas. Geological Journal, 21, 225-255.

Damuth, J. E., 1994, Neogene gravity tectonics and depositional processes on the deep Niger Delta continental margin: Marine and Petroleum Geology, 11, 321-346.

Davies, R.K., An, L., Medwedeff, D.A. and Yarwood, D., 2003. Structural Trap and Fault-seal Analysis, Offshore Myanmar: A Case Study. In: Duppenbecker, S. and Marzi, R. (eds.), Multidimensional basin modelling. AAPG/Datapages Discovery Series, 7, 157-173.

Dawers, N.H., Anders, M.H. and Scholz, C.H., 1993. Growth of normal faults: Displacement-length scaling. Geology, 21, 1107-1110.

Day-Stirrat, R.J., McDonnell, A. and Wood, L.J., 2010. Diagenetic and Seismic Concerns Associated with Interpretation of Deeply Buried 'Mobile Shales'. In: Wood, L. (ed.), Shale Tectonics, AAPG Memoir 93, 5-27.

Delisle G., Von Rad U., Andruleit H., Von Daniels C.H., Tabrez A.R. and Inam, A., 2002. Active mud volcanoes on- and offshore eastern Makran, Pakistan. International Journal of Earth Sciences, 91, 93-110.

Demercian, S., Szatmari, P. and Cobbold, R., 1993. Style and pattern of salt diapirs due to thin-skinned gravitational gliding, Campos and Santos basins, offshore Brazil. Tectonophysics, 228, 393 – 433.

De Vera, J., Granado, P. and McClay, K.R., 2009. Structural evolution of the Orange Basin gravity-driven system, offshore Namibia: Marine and Petroleum Geology, 27, 223–237.

Dooley, T., Ferguson, A., Poblet, J. and McClay, K., 2000. Tectonic evolution of the Sanga Sanga Block, Mahakam Delta, Kalimantan, Indonesia. AAPG Bulletin, 84, 6, 765-786.

Doust, H. and Omatsola, E., 1989. Niger Delta. AAPG Memoir, 48, 201-238.

Edwards, M. B., 1976. Growth faults in Upper Triassic deltaic sediments, Svalbard. AAPG Bulletin, 60, 341-355.

Edwards, M.B., 1995. Differential subsidence and preservation potential of shallow-water Tertiary sequences, northern Gulf Coast Basin, USA. In Plint, A. G. (ed.), Sedimentary facies analysis. International Association of Sedimentologists Special Publication 22, 265–281.

Eichhubl, P., Davatezes, N.C. and Becker, S., 2009. Structural and diagenetic control of fluid migration and cementation along the Moab Fault, Utah. AAPG Bulletin, 93, 653-681.

Ellis, G. and McClay, K.R., 1988. Listric extensional fault systems - results of analogue model experiments. Basin Research, 1, Issue 1, pages 55–70.

Ellouz-Zimmermann, N., Deville, E., Müller, C., Lallemant, S., Subhani, A.B. and Tabreez, A.R., 2007. Impact of sedimentation on convergent margin tectonics: example of the Makran accretionary prism (Pakistan). In: Lacombe, O., Roure, F., Lavé, J. and Vergés, J. (eds.),

Thrust Belts and Foreland Basins - From Fold Kinematics to Hydrocarbon Systems. Springer Verlag, Berlin, 327-350.

Evamy, D.D., Haremboure, J., Kamerling, P., Knapp, W.A., Molloy, F. A. and Rowlands, H., 1978. Hydrocarbon habitat of Tertiary Niger Delta: AAPG Bulletin, 62, 1–39.

Fazli Khani, H. and Back, S., 2012. Temporal and lateral variation in the development of growth faults and growth strata in the western Niger Delta, Nigeria. AAPG Bulletin, 96, 595-614.

Fazli Khani, H. and Back, S., 2015a. The influence of differential sedimentary loading on rollover and accommodation creation in deltas. Marine and Petroleum Geology, 59, 136-149.

Fazli Khani, H. and Back, S., 2015b. The influence of pre-existing structure on the growth of syn-sedimentary normal faults in a deltaic setting, Niger Delta. Journal of Structural Geology, 73, 18-32.

Fielding, C., 2015. Anatomy of falling-stage deltas in the Turonian Ferron Sandstone of the western Henry Mountains Syncline, Utah: Growth faults, slope failures and mass transport complexes. Sedimentology 62(1), 1-26.

Fruehn, J., White, R.S. and Minshull, T.A., 1997. Internal deformation and compaction of the Makran accretionary wedge. Terra Nova, 9, 101-104.

Fort, X., Brun, J. and Chauvel, F., 2004. Contraction induced by block rotation above salt (Angolan margin). Marine and Petroleum Geology, 21, 1281–1294.

Foxford, K.A., Walsh, J.J., Watterson, J., Garden, I.R., Guscott, S.C., and Burnley, S.D., 1998. Structure and content of the Moab Fault Zone, Utah, USA, and its implications for fault seal prediction. Geological Society of London, Special Publications, 147, 87-103.

Garfunkel, Z., 1984. Large-scale submarine rotational slumps and growth faults in the eastern Mediteranean. Marine Geology, 55, 305-324.

Ge, H., Jackson, M.P.A. and Vendeville, B.C., 1997. Kinematics and dynamics of salt tectonics driven by progradation. AAPG Bulletin, 81, 398-423.

Gawthorpe, R.L., Fraser, A.J., Collier, R.E.L., 1994. Sequence stratigraphy in active extensional basins: implications for the interpretation of ancient basin fills. Marine and Petroleum Geology, 11, 642 – 658.

Grando, G. and McClay, K., 2006. Morphotectonics domains and structural styles in the Makran accretionary prism, offshore Iran. Sedimentary Geology, 196, 157–179.

Guillaume, B., Dhont, D. and Brusset, S., 2008. Three-dimensional geologic imaging and tectonic control on stratigraphic architecture: Upper Cretaceous of the Tremp Basin (south-central Pyrenees, Spain). AAPG Bulletin, 92, 2, 249-269.

Hafid, M., Tari, G., Bouhadioui, D., El Moussaid, I., Echarfaoui, H. Ait Salem, A., Nahim, M. and Dakki, M.,2008. Atlantic Basins. In: Michard, A., Saddiqi, O., Chalouan, A. and Frizon de Lamotte, D. (eds), Continental Evolution: The Geology of Morocco, Springer, Berlin, 303-330.

Hardin, F.R. and Hardin, G.C., 1961. Contemporaneous normal faults of Gulf Coast and their relation to flexures, AAPG Bulletin, 45, 238-248.

Harms, J.C., Cappel, H.N. and Francis, D.C., 1984. The Makran coast of Pakistan: Its stratigraphy and hydrocarbon potential. In: Haq, B.U. and Milliman, J.D. (eds.), Marine Geology and Oceanography of Arabian Sea and Coastal Pakistan. VNRC, New York, 3-27.

Hesse, S., Back, S. and Franke, D., 2009. The deepwater fold–thrust belt offshore NW Borneo: gravity-driven vs. basement-driven shortening. Geological Society of America Bulletin, 121, 939–953.

Hesse, S., Back, S. and Franke, D., 2010. The structural evolution of folds in a deepwater fold and thrust belt - a case study from the Sabah continental margin offshore NW Borneo, SE Asia. Marine and Petroleum Geology, 27, 442-454.

Hiscott, R. N., 2003. Latest Quaternary Baram Prodelta, NW Borneo. In Sidi, F.H., Nummedal, D., Imbert, P., Darman, H. and Posamentier, H.W. (eds.), Tropical Deltas of Southeast Asia - Sedimentology, Stratigraphy, and Petroleum Geology: Society for Sedimentary Geology (SEPM), Special Publication, 76, 89-107.

Hodgetts, D., Imber, J., Childs, C., Flint, S., Howell, J., Kavanagh, J., Nell and Walsh, J., 2001. Sequence stratigraphic responses to shoreline-perpendicular growth faulting in shallow

marine reservoirs of the champion field, offshore Brunei Darussalam, South China Sea. AAPG Bulletin, 85, 433- 457.

Hooper, R.J., Fitzsimmons, R.J., Grant, N. and Vendeville, B.C., 2002. The role of deformation in controlling depositional patterns in the south- central Niger Delta, West Africa: Journal of Structural Geology, 24, 847-859.

Hunting Survey Cooperation Ltd., 1960. Reconnaissance Geology of Part of West Pakistan. Maracle Press, Oshawa, Ontario, Canada, 550 p.

Imber, J., Childs, C., Nell, A.R., Walsh, J.J., Hodgetts, D. and Flint, S., 2003. Hanging wall fault kinematics and footwall collapse in listric growth fault systems. Journal of Structural Geology, 25, 197-208.

Ings, S.J. and Beaumont, C., 2010. Continental margin shale tectonics: preliminary results from coupled fluid-mechanical models of large-scale delta instability. Journal of the Geological Society, London, 167, 571-582.

Jackson, M.P.A. and Galloway, W.E. 1984. Structural and depositional styles of Gulf Coast Tertiary continental margins: application to hydrocarbon exploration. AAPG Continuing education course notes series, 25, 226 p.

Jackson, C.A.L., Gawthorpe, R.L. and Sharp, I.R., 2006. Style and sequence of deformation during extensional fault-propagation folding: examples from the Hamman Faraun and El-Qaa fault blocks, Suez Rift, Egypt. Journal of Structural Geology, 28, 519-535.

Jackson, C.A.L., Jackson, M.P.A. and Hudec, M.R., 2015. Understanding the kinematics of salt-bearing passive margins: A critical test of competing hypotheses for the origin of the Albian Gap, Santos Basin, offshore Brazil. GSA Bulletin, 127, 1730-1751.

Jackson, C.A.L., and E. Larsen, 2009. Temporal and spatial development of a gravity-driven normal fault array: Middle-Upper Jurassic, South Viking Graben, northern North Sea: Journal of Structural Geology, 31, 388– 402.

Kidston, A.G., Smith, B., Brown, D.E., Makrides, C. and Altheim, B., 2007. Nova Scotia Deep Water Offshore Post-Drill Analysis - 1982-2004. CNSOPB Halifax, Nova Scotia, 181 p.

Kim, Y.-S., and Sanderson, D.J., 2005. The relationship between displacement and length of faults: a review. Earth Science Reviews 68, 317-334.

Kuecher, G. J., Roberts, H. H., Thompson, M. D. and Matthews, I., 2002. Evidence for Active Growth Faulting in the Terrebonne Delta Plain, South Louisiana: Implications for Wetland Loss and the Vertical Migration of Petroleum. Environmental Geosciences, 8, 77–94.

Lawrence, S.R., Munday, S., Bray, R., 2002. Regional geology and geophysics of the eastern Gulf of Guinea (Niger Delta to Rio Muni). The Leading Edge, 21, 1112–1117.

Leduc, A.M., Davies, R.J., Densmore, A.L. and Imber, J., 2012. The lateral strike-slip domain in gravitational detachment delta systems: A case study of the northwestern margin of the Niger Delta. AAPG Bulletin, 96, 709–728

Legett, J.K. and Platt, J., 1984. Structural features of the Makran Fore-arc on Landsat Imagery. In: Haq, B. U. and Milliman, J. D. (Editors), Marine Geology and Oceanography of Arabian Sea and Coastal Pakistan. VNRC, New York, 33-43.

Lewis, G., Knipe, R.J. and Li, A., 2000. Fault seal analysis in unconsolidiated sediments: a field study from Kentucky, USA. In Koestler, A.G. and Hunsdale, R. (eds.), Hydrocarbon Seal Quantification, Norsk Petroleumsforening, 11, 243-253.

Lopez, J.A., 1990. Structural styles of growth faults in the U.S. Gulf Coast Basin. In Brooks, F. (ed.), Classic Petroleum Provinces: Geological Society of London, Special Publication, 50, 203-219.

Lowell, J.D., 1985. Structural Styles in Petroleum Exploration. OGCI Publications, Tulsa. 26-31 and 351-392.

Lundin, E. R., 1992. Thin-skinned extensional tectonics on a salt detachment, northern Kwanza Basin, Angola: Marine and Petroleum Geology, 9, 405-411.

Mahanjane, E. and Franke, D., 2014. The Rouvuma Delta deep-water fold-and-thrust belt, offshore Mozambique. Tectonophysics, 614, 91-99.

Manzocchi, T., Heath, A.E., Palananthakumar, B., Childs, C. and Walsh, J.J., 2008. Faults in conventional flow simulation models: a consideration of representational assumptions and geological uncertainties. Petroleum Geoscience, 14, 91-110.

Martinsen, O.J., 1989. Styles of soft-sediment deformation on a Namurian (Carboniferous) delta slope, Western Irish Namurian Basin, Ireland. In: Whateley, M.K.G. and Pickering, K.T. (eds), Deltas: Sites and Traps for Fossil Fuels. Geological Society London, Special Publication, 41, 167-177.

Mauduit, T. and Brun, J., 1998. Growth fault/rollover systems: Birth, growth, and decay. Journal of Geophysical Research, 103, B8, 18119-18136.

McCall, G.J.H. and Kidd, R.G.W., 1982. The Makran southeastern Iran: the anatomy of a convergent margin active from Cretaceous to present. In: Leggett, J.K. (ed.) Trench-forearc geology: Sedimentation and tectonics on modern and ancient active plate margins: Geological Society London, Special Publication, 10, 387–397.

McClay, K.R., Waltham, D.A., Scott, A.D. and Abousetta, A., 1991. Physical and seismic modelling of listric normal faults. In: Roberts, A. M., Yielding, G. and Freeman, B. (eds.), The Geometry of Normal Faults, Geological Society of London Special Publication, 56, 231-239.

McClay, K., Munoz, J.-A., Garcia-Senz, J., 2004. Extensional salt tectonics in a contractional orogen: A newly identified tectonic event in the Spanish Pyrenees. Geology, 32; 9; 737–740.

McCulloh, R., 1988. Differential fault-related early Miocene sedimentation, Bayou Herbert area, southwestern Louisiana: AAPG Bulletin, 72, 477–492.

McDonnell, A., Jackson, M. A. and Hudec, M.R., 2010. Origin of transverse folds in an extensional growth-fault setting: Evidence from an extensive seismic volume in the western Gulf of Mexico. Marine and Petroleum Geology, 27, 1494-1507.

Modica, C.J. and Brush, E.R., 2004. Postrift sequence stratigraphy, paleogeography, and fill history of the deep-water Santos Basin offshore southeast Brazil. AAPG Bulletin, 88, 923-945.

Mora-Glukstad, M., Diaz, E., Maili, E. and Martinez, P., 2003. Case study of an integrated geophysical and structural analysis of the prolific Vivian sandstones in the Northern Marañón Basin, Perú. The Leading Edge, 22, 1148-1156.

Morley, C. K., and Guerin, G., 1996, Comparison of gravity-driven deformation styles and behavior associated with mobile shales and salt: Tectonics, 15, 1154-1170.

Morley, C.K., Crevello, P. and Zulkifli Haji Ahmad, 1998. Shale tectonics and deformation associated with active diapirism: the Jerudong Anticline, Brunei Darussalam. Journal of the Geological Society, London, 155, 475–495.

Morley, C.K., Back, S., Van Rensbergen, P., Crevello, P. and Lambiase, J.J., 2003, Characteristics of repeated, detached, Miocene-Pliocene tectonic inversion events, in a large delta province on an active margin, Brunei Darussalam, Borneo. Journal of Structural Geology, 25, 1147–1169.

Morley, C.K., 2007. Interaction between critical wedge geometry and sediment supply in a deep-water fold belt. Geology, 35, 139-142.

Morley, C. K., King, R., Hillis, R., Tingay, M. and Backe, G., 2011. Deepwater fold and thrust classification, tectonics, structure and hydrocarbon prospectivity: A Review. Earth Science Reviews, 104, 41-91.

Morosanu, I.C., 1998. Extensional tectonics in the Tertiary of the Black Sea shelf – Romanian Offshore. Geo-Eco-Marina, 3, 153-158.

Nemec, W., Steel, R. L., Gjelberg, J., Collinson, J. D., Prestholm, E. and Øxnevad, I. E., 1988: Anatomy of a collapsed and reestablished delta front in the Lower Cretaceous of eastern Spitsbergen; Rotational sliding and sedimentation processes. AAPG Bulletin 72, 454-476.

Ocamb, R.D., 1961. Growth faults of south Louisiana. Gulf Coast Association Geological Socities Transactions, 11, 139-175.

Odling, N.E., Gillespie, , Bourgine, B., Castaing, C., Chiles, J.-, Christensen, N., Fillion, E., Genter, A., Olsen, C., Thrane, L., Trice, R., Aarseth, E., Walsh, J.J. and Watterson, J., 1999.

Variations in fracture system geometry and their implications for fluid flow in fractured hydrocarbon reservoirs. Petroleum Geoscience, 5, 373-384.

Osmundsen, T., Braathen, A., Rød, R.S. and Hynne, I.B., 2014: Styles of normal faulting and fault-controlled sedimentation in the Triassic deposits of Eastern Svalbard. Norwegian Petroleum Directorate Bulletin, 11, 61-69.

Ouillon, G., Sornette, D. and Castaing, C., 1995. Organisation of joints and faults from 1 cm to 100 km scales revealed by Optimization Anisotropic Wavelet Coefficient Method and multifractal analysis. Non-linear Processes in Geophysics, 2, 158-177.

Page, W.D., Alt, J.N., Cluff, L.S. and Plafker, G., 1979. Evidence for the recurrence of large magnitude earthquakes along the Makran Coast of Iran and Pakistan. Tectonophysics, 52, 533–547.

Paton, D.A, van der Spuy D., di Primio R. and Horsfield B., 2008. Tectonically induced adjustment of passive-margin accommodation space; influence on the hydrocarbon potential of the Orange Basin, South Africa, AAPG Bulletin, 92, 589-609.

Petersen, K., Clausen, O. R. and Korstgard, J. A., 1992. Evolution of a salt-related listric growth fault near the D-1 well, block 5605, Danish North Sea: displacement history and salt kinematics. Journal of Structural Geology, 14, 5, 565-577.

Platt, J., Legett, J.K., Young, J., Raza, H. and Alam, S., 1985. Large-scale sediment underplating in the Makran accretionary prism, southwest Pakistan. Geology, 13, 507-511.

Platt, J., Legett, J.K. and Alam, S., 1988. Slip vectors and fault mechanics in the Makran accretionary wedge, SW Pakistan. Geology, 13, 507-511.

Pochat, S., Castelltort, S., Van Den Driessche, J., Besnard, K. and C. Gumiaux, 2004. A simple method of determining sand/shale ratios from seismic analysis of growth faults: an example from upper Oligocene to lower Miocene Niger Delta deposits: AAPG Bulletin, 88, 1357-1367.

Pochat, S., Castelltort, S., Choblet, G. and Van Den Driessche, J., 2009. High-resolution record of tectonic and sedimentary processes in growth strata. Marine and Petroleum Geology, 26, 1350-1364.

Prestholm, E. and Walderhaug, O., 2000. Synsedimentary faulting in a Mesozoic deltaic sequence, Svalbard, Arctic Norway-fault geometries, faulting mechanisms, and sealing properties, AAPG Bulletin, 84, 505-522.

Quayyum, M., Niem, A.R. and Lawrence, R.D., 1996. Newly discovered Paleogene deltaic sequence in the Katawaz basin, Pakistan, and its tectonic implications. Geology, 24, 835-838.

Raza, H.A., Ahmed, R. and Ali, S.M., 1990. Pakistan offshore: an attractive frontier. Pakistan Journal of Hydrocarbon Research, 2, 1-42.

Rotevatn, A. and Jackson, C.A.L,. 2014. 3D structure and evolution of folds during normal fault dip linkage, Journal of the Geological Society of London, 171, 821-829.

Rouby, D. and Cobbold, R., 1996. Kinematic analysis of a growth fault system in the Niger Delta from restoration in map view. Marine and Petroleum Geology, 13, 565-580.

Rouby, D.,Raillard, S., Guillocheau, F.,Bouroullec, R.and Nalpas, T., 2002. Kinematics of a growth fault/raft system from restoration in 3D (West African Margin). Journal of Structural Geology, 24, 783-796.

Rouby, D., Guillocheau, F., Robin, C., Bouroullec, R., Raillard, S., Castelltort, S. and Nalpas, T., 2002. Rates of deformation of an extensional growth fault/raft system (offshore Congo, West African margin) from combined accommodation measurements and 3-D restoration. Basin Research, 15, 183-200.

Rykkelid, E. and Fossen, H., 2002. Layer rotation around vertical fault overlap zones: observations from seismic data, field examples and physical experiments. Marine and Petroleum Geology, 19, 181-192.

Sandal, S.T., 1996. The Geology and Hydrocarbon Resources of Negara Brunei Darussalam: Seria, Brunei Darussalam, Brunei Shell Petroleum Company, 243 p.

Saller, A. and Blake, G., 2003. Sequence stratigraphy and syndepositional tectonics of Upper Miocene and Pliocene deltaic sediments, offshore Brunei Darussalam. In Sidi, F.H., Nummedal, D., Imbert, P., Darman, H. and Posamentier, H.W. (eds.), Tropical Deltas of

Southeast Asia - Sedimentology, Stratigraphy, and Petroleum Geology: Society for Sedimentary Geology (SEPM), Special Publication, 76, 219-234.

Sapin, F., Ringenbach, J.-C., Rives, T. and Pubellier, M., 2012. Counter-regional normal faults in shale-dominated deltas: Origin, mechanism and evolution. Marine and Petroleum Geology, 37, 121-128.

Satyana, A.H., Nugroho, D. and Surantoko, I., 1999. Tectonic controls on the hydrocarbon habitats of the Barito, Kutei, and Tarakan Basins, Eastern Kalimantan, Indonesia: major dissimilarities in adjoining basins. Journal of Asian Earth Sciences, 17, 99-122.

Sestini, G., 1989. Nile Delta, a review of depositional environments and geological history, in M. K. G. Whateley and K. T. Pickering, Deltas, Sites and Traps for Fossils Fuels: Special Publication of Geological Society of London, 41, 99-127.

Schlische, R.W., 1991. Half-graben basin filling models: New constraints on continental extensional basin development. Basin Research, 3, 123-141.

Shipton, Z.K., Soden, A.M., Kirkpatrick, J.D., Bright, A.M. and Lunn, R.J., 2006. How thick is a Fault? Fault displacement-thickness scaling revisited. Earthquakes: Radiated Energy and the Physics of Faulting, AGU Geophysical Monograph Series 170, 193-198.

Shultz, M.R. and Hubbard, S.M., 2005. Sedimentology, stratigraphic architecture, and ichnology of gravity-flow deposits partially ponded in a growth-fault controlled slope minibasin, Tres Pasos Formation (Cretaceous), southern Chile. Journal of Sedimentary Research, 75, 3, 440-453.

Snead, R.J., 1993. Uplifted marine terraces along the Makran coast of Pakistan and Iran. In: Shroder Jr., J.F. (ed.), Himalaya to the Sea. Routledge, London, 327–362.

Tachikawa, T., Hato, M., Kaku, M. and Iwasaki, A., 2011. Characteristics of ASTER GDEM Version 2. IGARRS 2011, Vancouver, Canada. Session: TH2.T05.3.

Tari, G. Kohazy, R., Hannke, K, Hussein, H., Novotny, B. and Mascle, J., 2012. Examples of deep-water play types in the Matruh and Herodotus basins of NW Egypt. The Leading Edge, 31, 816-823.

Taylor, S.K., Nicol,, A. and Walsh, J.J., 2008. Displacement loss on growth faults due to sediment compaction. Journal of Structural Geology, 30, 394-405.

Terzaghi, K., 1956. Varieties of submarine slope failures. Proceedings of the 8th Texas Conference on Soil Mechanics and Foundation Engineering, University of Texas, Bureau of Engineering Research, Special Publication, 29, 40 p.

Thorsen, C. E., 1963, Age of growth faulting in southeast Louisiana: Gulf Coast Association of Geological Societies Transactions, 13, 103–110.

Tinker, J., de Wit, M. and Grotzinger, J., 2002. Seismic Stratigraphic Constraints on Neoarchean-Paleoproterozoic Evolution of the Western Margin of the Kaapvaal Craton, South Africa. South African Journal of Geology, 105, 107-134.

Totterdell, J.M., and Krassay, A.A., 2003. The role of shale deformation and growth faulting in the Late Cretaceous evolution of the Bight Basin, offshore southern Australia. In: Van Rensbergen, et al. (eds.), Subsurface Sediment Mobilization, Geological Society London, Special Publication, 41, 429–442.

Treviño, R.H., and Vendeville, B.C., 2008. Origin of coast-perpendicular extensional faults, western Gulf of Mexico: the relationship between an early-stage ridge and a late-stage fault. AAPG Bulletin, 92, 951-964.

Trudgill, B. and Cartwright, J., 1994. Relay-ramp forms and normal-fault linkages, Canyonlands National Park, Utah. Geological Society of America Bulletin, 106, 1143-1157.

Trudgill, B., 2015. Unraveling the Geometry and Origin of a Northeast-Southwest Striking Linked Fault Array at Marshall Mesa, Western Denver Basin: A Solution Through Integrated Digital Mapping. AAPG Annual Convention and Exhibition, Denver, Abstract 2106330.

Tvedt A.B.M., Rotevatn A., Jackson C.A.L., Fossen H., Gawthorpe R.L., 2013. Growth of normal faults in multilayer sequences: A 3D seismic case study from the Egersund Basin, Norwegian North Sea. Journal of Structural Geology, 55, 1-20.

Van der Zee, W., and Urai, J.L., 2005. Processes of normal fault evolution in a siliciclastic sequence: A case study from Miri, Sarawak, Malaysia: Journal of Structural Geology, 27, 2281–230.

Van Rensbergen, P. and Morley, C., 2000. 3-D seismic study of a shale expulsion syncline at the base of the Champion Delta, offshore Brunei, and its implications for the early structural evolution of large delta systems. Marine and Petroleum Geology, 17, 861–872.

Volozh, Y., Talbot, C. and Ismail-Zadeh, A., 2003. Salt structures and hydrocarbons in the Pricaspian basin. AAPG Bulletin, 87, 2, 313-334.

Vredenburg, E.W., 1909. Report on the geology of Sarawan, Jhalawan, Mekran and the state of Las Bela, considered principally from the point of view of economic development. Rec. Geol. Sur India, 3,189–215.

Wade , J.A. and McLean, B.C., 1990. The geology of the southeastern margin of Canada. In Keen, M.J. and Williams, G.L. (eds), Geology of the Continental Margin of Eastern Canada. Geological Survey of Canada, Geology of Canada, 2, 167–238.

Walsh, J.J. and Watterson, J., 1988. Analysis of the relationship between displacements and dimensions of faults. Journal of Structural Geology, 15, 1509-1512.

Walsh, J.J., Watterson, J., Bailey, W.R., Childs, C., 1999. Fault relays, bends and branch-lines. Journal of Structural Geology, 21, 1019-1026.

White, R.S., 1983. The Makran accretionary prism. In: Bally, A.W. (ed.), Seismic Expression of Structural Styles. AAPG Studies in Geology, vol. 15. 3.4.2-178 to 3.4.2-182.

Wignall, B. and Best, J. L. 2004. Sedimentology and kinematics of a large, retrogressive growth-fault system in Upper Carboniferous deltaic sediments, western Ireland, Sedimentology, 51, 1343-1358.

Winker, C.D. and Edwards, M.B., 1983. Unstable progradational clastic shelf margins. In: Stanley, D.J. and Moore, G. (eds.), The Shelf Break: Critical Interface on Continental Margins, SEPM Special Publication, 33, 139-157.

Wood, L.J., 2000. Chronostratigraphy and Tectonostratigraphy of the Columbus Basin, Eastern Offshore Trinidad. AAPG Bulletin, 84, 12, 1905-1928.

Zecchin, M., Massari, F., Mellere, D. and Prosser, G., 2003. Architectural styles of prograding wedges in a tectonically active setting, Crotone Basin, Southern Italy. Journal of the Geological Society, London, 160, 863–880.

Zecchin, M., Massari, F., Mellere, D. and Prosser, G., 2004. Anatomy and evolution of a Mediterranean-type fault bounded basin: the Lower Pliocene of the northern Crotone Basin (Southern Italy). Basin Research, 16, 117–143.

Zecchin, M., 2005. Relationships between fault-controlled subsidence and preservation of shallow-marine small-scale cycles: example from the lower Pliocene of the Crotone Basin (southern Italy). Journal of Sedimentary Research, 75, 300–312.

Zecchin, M., Mellere, D. and Roda, G., 2006. Sequence stratigraphy and architectural variability in growth fault-bounded basin fills: a review of Plio-Pleistocene stratal units of the Crotone Basin, southern Italy. Journal of the Geological Society, London, 163, 471–486.

Zhang, K.-J., Xia, B.-D., Wang, G.-M., Li, Y.-T. and Ye, H.F., 2004. Early Cretaceous stratigraphy, depositional environments, sandstone provenance, and tectonic setting of central Tibet, western China. GSA Bulletin, 116, no. 9/10, 1202–1222.

Zheng, W. and Deng, H., 2012. High-resolution sequence stratigraphic division and distribution of tidal deposits in the Zhuhai Formation, Huizhou Sag, Pearl River Mouth Basin, South China Sea. Geological Magazine, 149, 4, 722–728.

Figure Captions

Figure 1: Digital elevation map (DEM) of the world, showing locations of growth faults recorded on seismic-reflection data (white circles) and growth faults in outcrop (yellow circles). DEM from http://www.ngdc.noaa.gov.

Figure 2: Overview map (inset) and Landsat ETM+ image of the Pakistan part of the Makran fold and thrust belt and the coastal foreland from the Dasht River between Chabahar and Gwadar to the Sonmiani Bay north of Karachi. The coastal areas of the Makran fold and thrust belt expose spectacular folds, faults, and intensively folded and faulted strata of a major palaeo-delta (e.g. Quayyum et al. 1996; Carter et al. 2010). Black box indicates the location of the study area and of Figure 3. TR = Talar Formation.

Figure 3: Geological map of the study area (A), and Landsat ETM+ images of the Talar Syncline (B) and the Buzi Range outcrop succession of the Hingol area (C). The Neogene to

recent sedimentary succession of the Makran foreland can be subdivided into four major lithostratigraphic units: 1) the Panjgur Formation, 2) the Parkini Formation, 3) the Talar Formation, and 4) the Chatti, Ormara and Jiwani Formations. Geological overview after CPCP (1958), microfossil sample sites from Ellouz-Zimmermann et al. (2007). Black boxes in geological map (A) indicate locations of satellite images (B) and (C).

Figure 4: Stratigraphic chart of this study, and statigraphic subdivision of Ellouz-Zimmermann et al. (2007), Critelli et al. (1990), Ahmed (1969) and CPCP (1958). The focus of this study is the late Miocene to Pliocene Talar Formation.

Figure 5: Monochromatic SPOT satellite image of the central part of the Buzi Range, horizontally mirrored and counter-clockwise (CCW) rotated by 200°. The rotation and mirroring places the satellite data into stratigraphic order (old deposits = bottom; young deposits = top); the regional westward-oriented transport direction of the sedimentary system is on the left side of the figure. All satellite data presented in the following are plotted the same way. (A) SPOT image blended with an ASTER digital elevation model, (B) SPOT data overlain by fault and horizon interpretation, and (C) geological image interpretation. The NW-SE trending sandstone-shale succession is exposed over a length of 20 km at elevations between 100 and 450 m; the outcrop-width perpendicular to the bedding is over 6 km, which equals approximately 4 km of true stratigraphic thickness (TST) after dip and topography correction.

Figure 6: Relative chronostratigraphy of growth faulting in the central part of the Buzi Range, documenting a general landward backstepping of counter-regional growth faulting, hanging-wall bending and collapse through time. Stratal bending at horizon-8-level in the hanging wall of fault F4 can be attributed to late-stage depositional loading of the sandstone-shale succession with massive, amalgamated sandstones. This loading affects only the hanging wall of faults F3 and F4; faults F1 and F2 remain unaffected by late-stage loading.

Figure 7: 200° rotated (CCW) and horizontally mirrored monochromatic SPOT satellite image of the northwestern part of the Talar Syncline blended with an ASTER digital elevation model (A), overlain by a fault and horizon interpretation (B), and geological image interpretation (7C). The WSW-trending sandstone-shale succession is imaged along a > 60 km long section that lies at elevations between 50 and 800m. The outcrop-width perpendicular to bedding is in places > 12 km, which equals > 8 km of true stratigraphic thickness (TST) after dip and topography correction.

Figure 8: 20° clockwise (CW) rotated monochromatic SPOT satellite image of the southwestern Talar Syncline blended with an ASTER digital elevation model (A), overlain by a fault and horizon interpretation (B), overview geological interpretation (C) and a detailed structural interpretation of the fault zone between faults X1 and X2 (D). The WSW-trending sandstone-shale succession is imaged along a section ca. 30 km long, exposed at elevations between 50 and 300 m. The outcrop-width perpendicular to the bedding is in places 10 km, which equals to ca. 3.5 km of true stratigraphic thickness (TST) after dip and topography correction.

Figure 9: 15° CW rotated monochromatic SPOT satellite image of the southeastern Talar Syncline (A) converted into true stratigraphic thickness (TST), imaging numerous, dominantly normal faults displacing the zone of maximum stratal bending (sandstone- and siltstone-dominated lithology = dark colors; mudstone-dominated lithology = light colors). (B) shows a fault and horizon interpretation, documenting horizon offset by synthetic and antithetic faults between a few metres up to 200 m. (C) is a conversion of the SPOT satellite image into pseudo-reflectivity data using the surface-lithology information as relative impedance estimate. Downward mudstone-sandstone contacts are defined as a relative impedance increase, corresponding to a seismic trough (red). The pseudo-reflectivity data is filtered to a synthetic frequency of 10 to 40 Hz (resolution of ca. 20 m). (D) provides for comparison a real-world, medium-resolution seismic-reflection section (zero-phase; European polarity; frequency 5 to 60 HZ) and well data across a deltaic rollover with a collapsed crest from the Niger Delta.

Figure 10: Synoptic view of rotated and horizontally mirrored SPOT image of the northern Talar Syncline succession (A) and the major Plio-Pleistocene Perdana-Frigate depocentre offshore NW Borneo (B). The Perdana-Frigate depocentre is bound in the west by the counter-regional Perdana-Frigate fault, a syn-sedimentary normal fault with up to a few kilometres displacement that extends laterally over more than 50 km (Morley, 2007). Note distinct similarities in the gross structural geometry and internal stratigraphic architecture of the fill of the offshore Borneo and onshore Pakistan depocentres. Black box in (A) shows location of Figures 11A and B, black box in (B) shows approximate location of flattened seismic image shown in Figure 11D.

Figure 11: Close-up of the sandstone-shale units at the base of the northern Talar Syncline in SPOT-image and pseudo-reflectivity display (A, B, C) compared to a flattened zoom-in of the basal clinoforms of the Perdana-Frigate depocenter offshore NW Borneo (D). The westward-prograding clinoform succession of the Talar Syncline shows a pronounced

basinward thinning, and, at the clinoform topsets, a shift from depositional aggradation to downstepping with a continued seaward stepping of the sedimentary system (A, B). Note difference in resolution between onlap imaged on SPOT data and in pseudo-reflectivity display (C). A comparable scenario can be interpreted from the 2D seismic-reflection section of the Perdana-Frigate depocentre (D), where stacks of prograding clinoforms precede the formation of a basinward thickening, fault-controlled wedge in the hanging wall of the major western bounding fault.

Figure 12: (A) Schematic illustration of a purely sediment-driven mechanism that could control the initiation of counter-regional growth faults in front of prograding clinoforms (Talar Syncline succession; Perdana-Frigate example), in which differential loading, compaction and fluid expulsion create synclines on the clinoform bottomsets that potentially trap turbidite and slope sediments. Further preferential, rapid sediment accumulation in such a loading-induced depocenter could lead to stratal rupture and fault initiation between the syncline fill and less compacted deposits basinward. A similar mechanism has been proposed for the Albian Gap, a large salt-tectonic structure offshore Brazil (Jackson et al., 2015). (B) Schematic illustration of a lithology-driven mechanism potentially controlling the initiation of counter-regional growth faults in the Buzi Range succession. The interpretation varies from (A) in that solely the nature of the pre-existing substratum initially controls the generation of space, which, when filled, differentially compacts and reacts to further loading until finally reaching a stable compaction state.

Figure 13: Seismic-reflection example of a slope depocenter offshore NW Borneo formed above a deeper-seated thrust hanging-wall anticline. Such depocentres can act in a similar way to their purely loading-initiated counterparts in compacting and subsiding more rapidly than their surroundings, potentially generating comparable fault and stratigraphic geometries. For the western part of the southern Talar Syncline (Figs. 7, 8), the possible presence of larger-scale, deep-seated, pre-existing thrust faults or shale movement/diapirism within the Parkini Shales cannot be excluded.

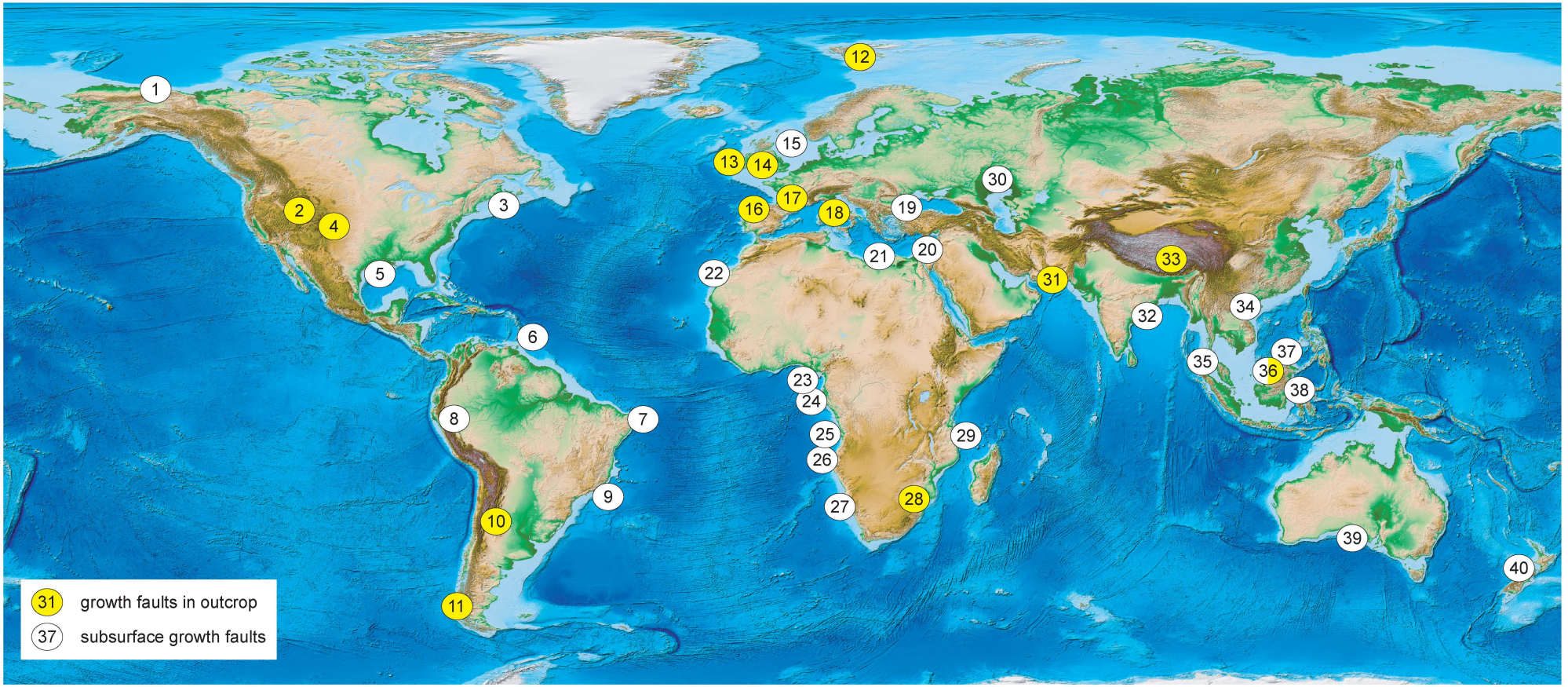

1	Alaska	Curtis (1986)
2	Utah	Trudgill & Cartwright (1994)
		Bhattacharya & Davies (2001)
		Fielding (2015)
3	Canada	Wade & McLean (1990)
		Cummings and Arnott (2005)
		Kidston et al. (2007)
4	Denver Basin	Trudgill (2015)
5	Texas + GOM	Lopez (1990)
		Edwards (1995)
		Cartwright et al. (1998)
		Kuecher et al. (2001)
		Brown et al. (2004)
		Treviño & Vendeville (2008)
		McDonnell et al. (2010)
		Olariu et al. (2013)
6	Trinidad	Wood (2000)
7	Amazon	Cobbold et al. (2004)
8	Peru	Mora-Glukstad et al. (2003)
9	Central Brazil	Demercian et al. (1993)
		Modica & Brush (2004)
10	Argentina	Albrecht (2005)
11	Chile	Shultz and Hubbard (2005)
12	Spitsbergen	Edwards (1976)
		Nemec et al. (1988)
		Prestholm and Walderhaug (2000)
13	Ireland	Martinsen (1989)
		Wignall & Best (2004)
14	UK	Chisholm & Waters (2012)
15	North Sea	Chapman and Meneilly (1991)
		Jackson and Larsen (2009)
		Petersen et al. (1992)
16	Spain	McClay et al. (2004)
		Guillaume et al. (2008)
17	France	Bouroullec et al. (2004)
18	Italy	Balsamo et al. (2008)
		Zecchin et al. (2003, 2004, 2005, 2006)
19	Romania	Morusanu (1998)
		Bega & Ionescu (2009)
20	Levant Basin	Baudon & Cartwright (2008)
21	Egypt	Sestini (1989)
		Beach & Tayner (1991)
		Tari et al. (2012)
22	Morocco	Hafid et al. (2008)
23	Nigeria	Doust & Omatsola (1990)
		Morley & Guerin (1996)
		Rouby and Cobbold (1996)
		Back et al. (2006)
		Pochat et al. (2004, 2009)
		Leduc et al. (2012)
		Fazli Khani & Back (2015a, b)
24	Gulf of Guinea	Lawrence et al. (2002)
25	Congo-Cabinda	Rouby et al. (2002, 2003)
		Chimey & Kluth (2002)
26	Angola	Fort et al. (2004)
		Lundin (1992)
27	Namibia & South Africa	Paton et al. (2008)
		DeVera et al. (2010)
		Butler & Paton (2010)
28	South Africa	Tinker et al. (2002)
29	Mozambique	Mahanjane & Franke (2014)
30	Kazakhstan	Volozh et al. (2003)
31	Pakistan	this study
32	India	Choudhuri et al. (2008)
33	Tibet	Zhang et al. (2004)
34	China	Zheng & Deng (2012)
35	Myanmar	Davies et al. (2003)
36	Brunei	Burhannudinnur and Morley (1997)
		Hodgetts et al. (2001)
		Imber et al. (2003)
		Morley et al. (2003)
		Back et al. (2005)
37	East Malaysia	Van der Zee & Urai (2005)
		Hesse et al. (2009, 2010)
		Sapin et al. (2012)
38	Kalimantan	Satyana et al. (1999)
		Dooley et al. (2000)
		Armandita et al. (2015)
39	South Australia	Totterdell & Krassay (2003)
40	New Zealand	Taylor et al. (2008)

Figure 1

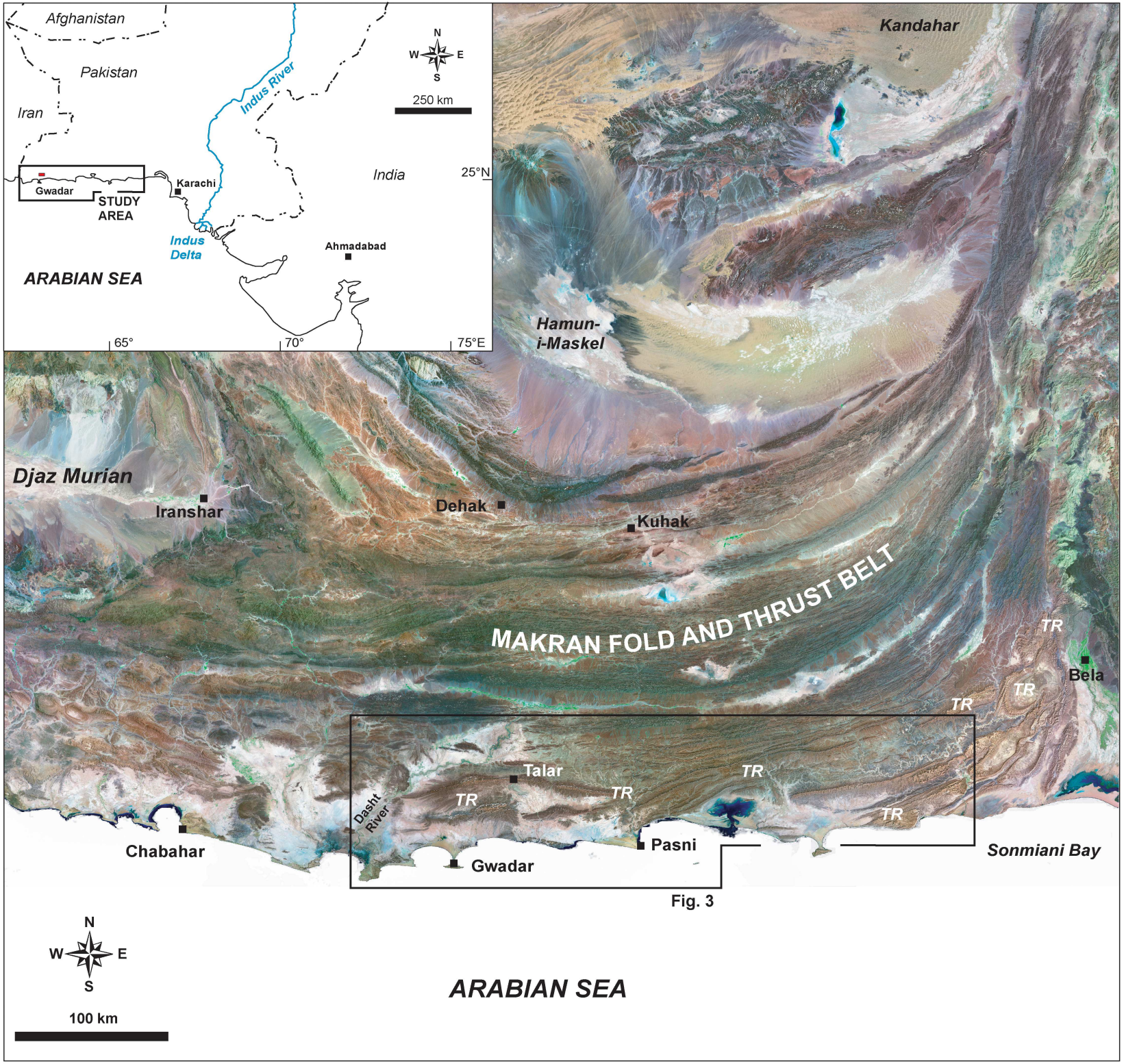
Afghanistan
Pakistan
Iran
Indus River
India
N
W
E
S
250 km
25°N
Gwadar
STUDY AREA
Karachi
Indus Delta
Ahmadabad
ARABIAN SEA
65°
70°
75°E
Kandahar
Hamun-i-Maskel
Djaz Murian
Iranshar
Dehak
Kuhak
MAKRAN FOLD AND THRUST BELT
TR
Bela
Talar
Dasht River
Pasni
Sonmiani Bay
Chabahar
Gwadar
Fig. 3
N
W
E
S
100 km
ARABIAN SEA

Figure 2

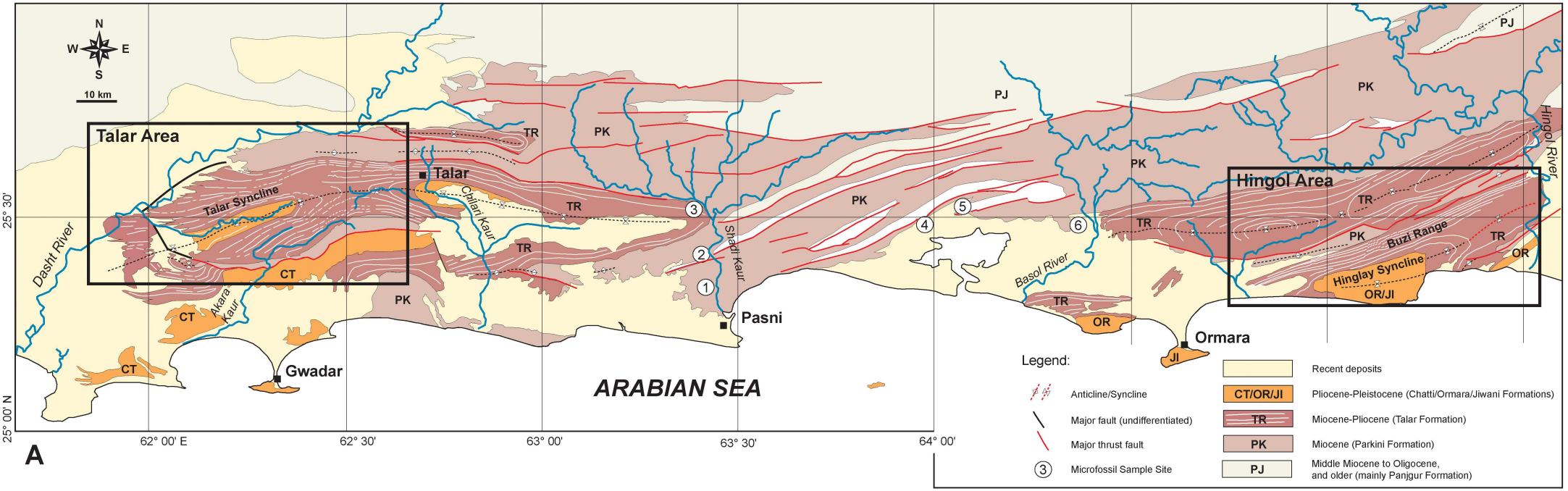
N
W
E
S
10 km
Talar Area
Talar
Talar Syncline
Dasht River
Chilari Kaur
Akara Kaur
Shadi Kaur
Basol River
Hingol River
Hingol Area
Buzi Range
Hinglay Syncline
OR/JI
Pasni
Ormara
Gwadar
ARABIAN SEA
PJ
PK
TR
CT
OR
JI
1
2
3
4
5
6
25° 30' N
25° 00' N
62° 00' E
62° 30'
63° 00'
63° 30'
64° 00'
Legend:
Recent deposits
Anticline/Syncline
CT/OR/JI
Pliocene-Pleistocene (Chatti/Ormara/Jiwani Formations)
Major fault (undifferentiated)
TR
Miocene-Pliocene (Talar Formation)
Major thrust fault
PK
Miocene (Parkini Formation)
Microfossil Sample Site
PJ
Middle Miocene to Oligocene, and older (mainly Panjgur Formation)

A

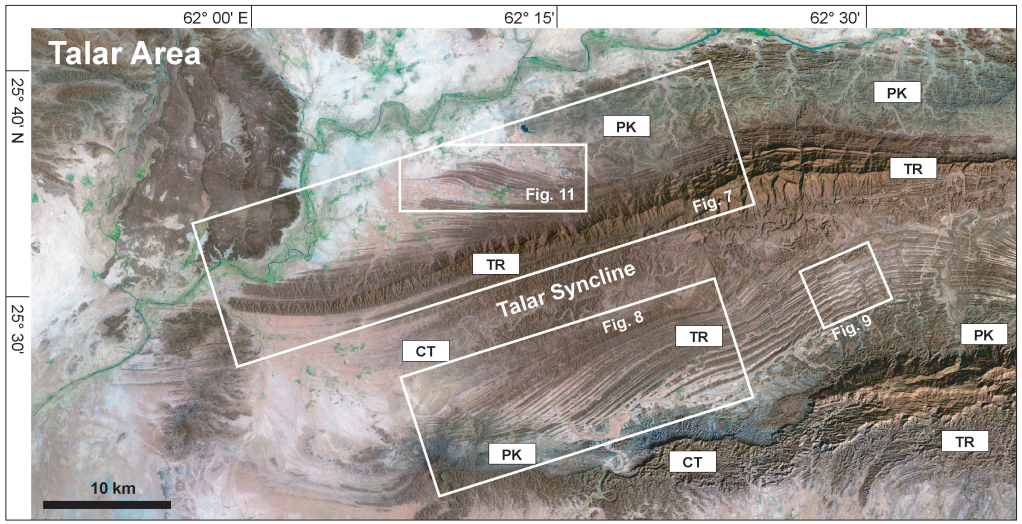
62° 00' E
62° 15'
62° 30'
Talar Area
25° 40' N
25° 30'
PK
TR
CT
Fig. 11
Fig. 7
Talar Syncline
Fig. 8
Fig. 9
10 km

B

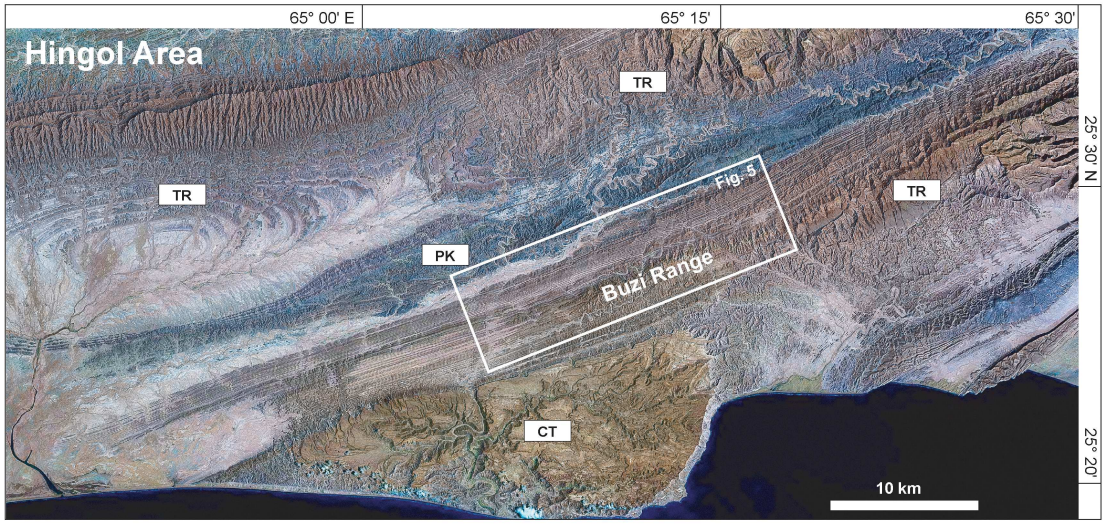
65° 00' E
65° 15'
65° 30'
Hingol Area
25° 30' N
25° 20'
TR
PK
CT
Fig. 5
Buzi Range
10 km

C

Figure 3

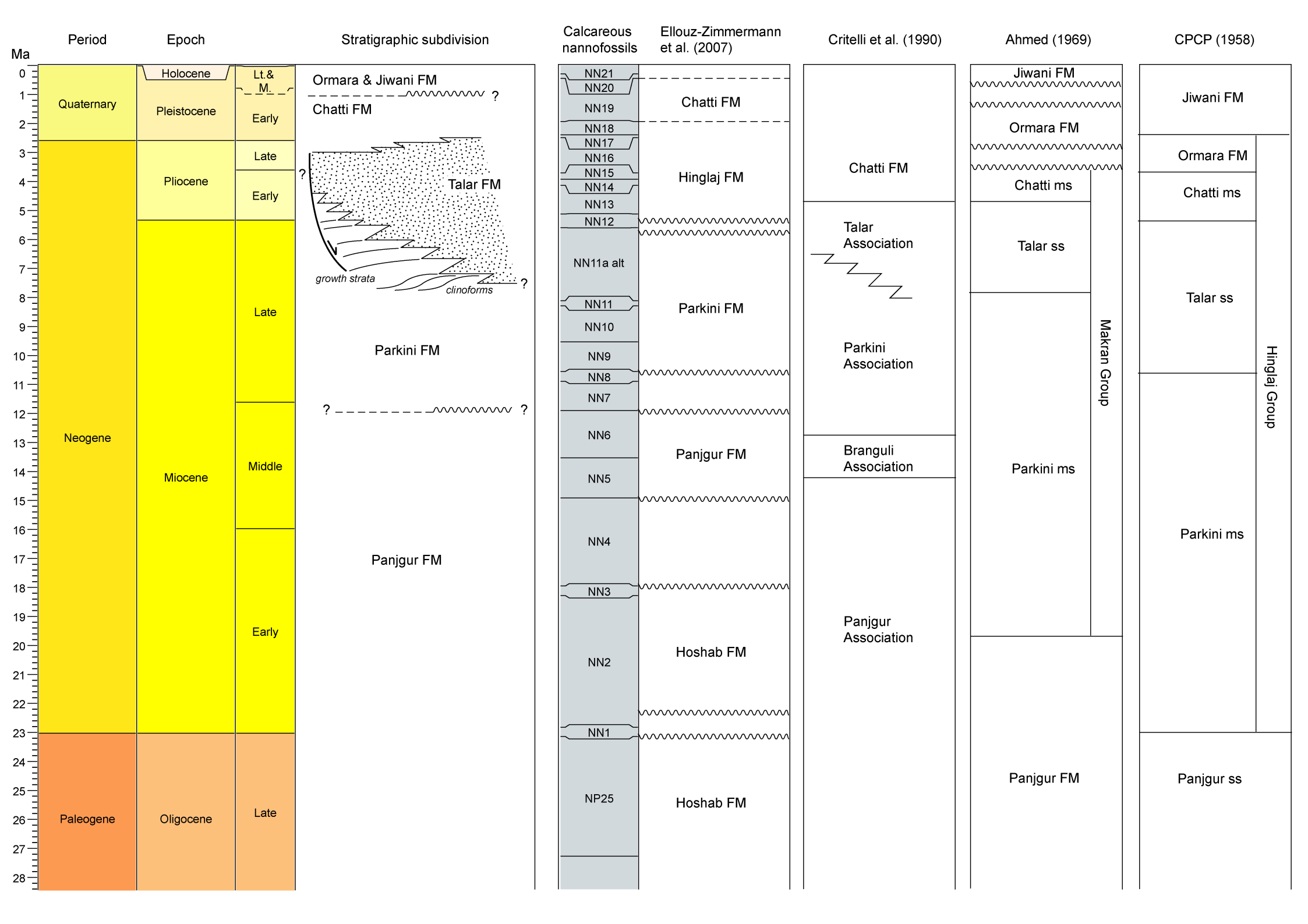
Ma
Period
Epoch
Stratigraphic subdivision
Calcareous nannofossils
Ellouz-Zimmermann et al. (2007)
Critelli et al. (1990)
Ahmed (1969)
CPCP (1958)
Quaternary
Neogene
Paleogene
Holocene
Pleistocene
Pliocene
Miocene
Oligocene
Lt.& M.
Early
Late
Middle
Ormara & Jiwani FM
Chatti FM
Talar FM
growth strata
clinoforms
Parkini FM
Panjgur FM
NN21
NN20
NN19
NN18
NN17
NN16
NN15
NN14
NN13
NN12
NN11a alt
NN11
NN10
NN9
NN8
NN7
NN6
NN5
NN4
NN3
NN2
NN1
NP25
Hinglaj FM
Hoshab FM
Talar Association
Parkini Association
Branguli Association
Panjgur Association
Jiwani FM
Ormara FM
Chatti ms
Talar ss
Parkini ms
Makran Group
Hinglaj Group
Panjgur ss

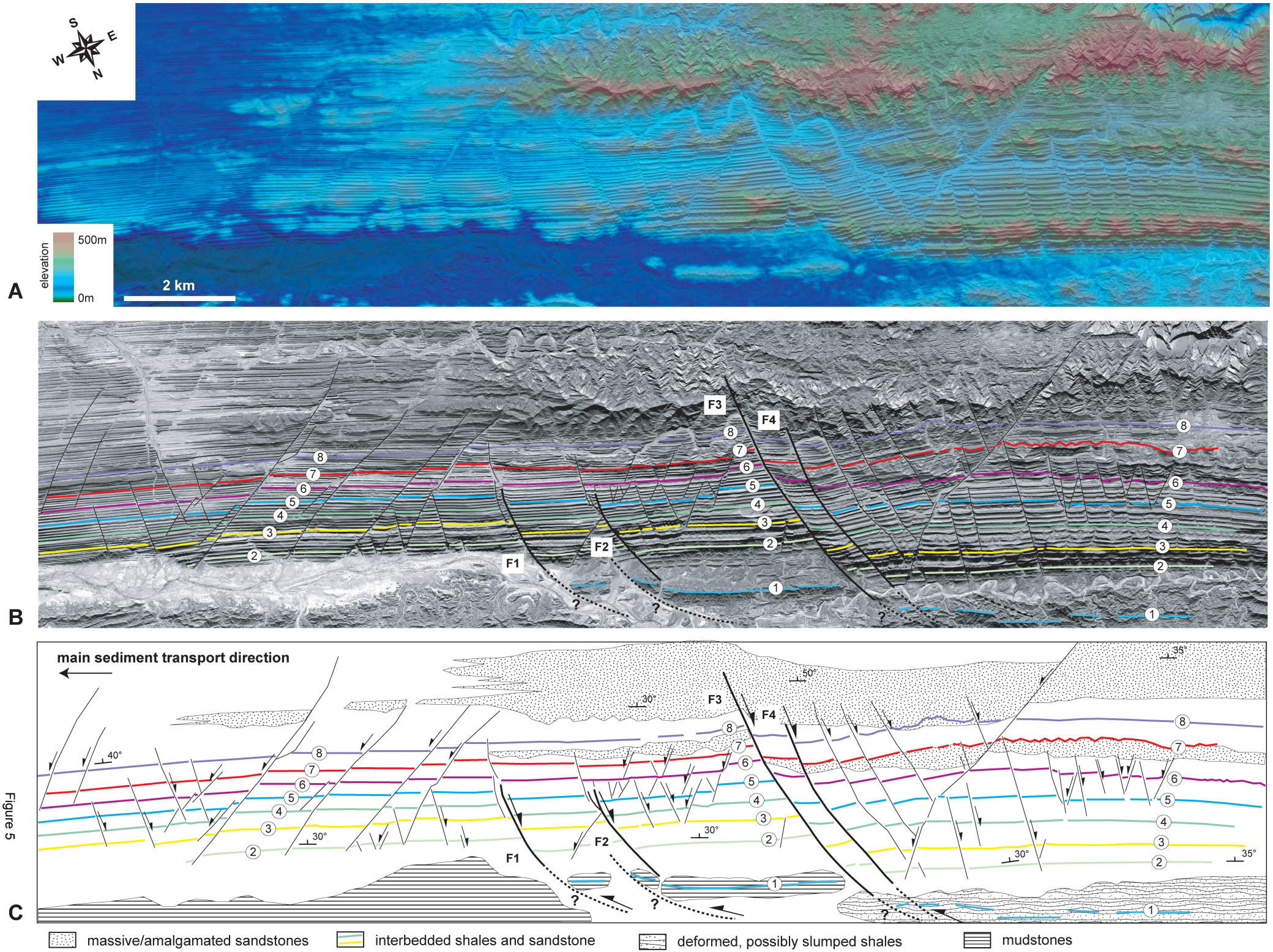
A
S
W
E
N
elevation
500m
0m
2 km
B
F1
F2
F3
F4
main sediment transport direction
C
massive/amalgamated sandstones
interbedded shales and sandstone
deformed, possibly slumped shales
mudstones

Figure 5

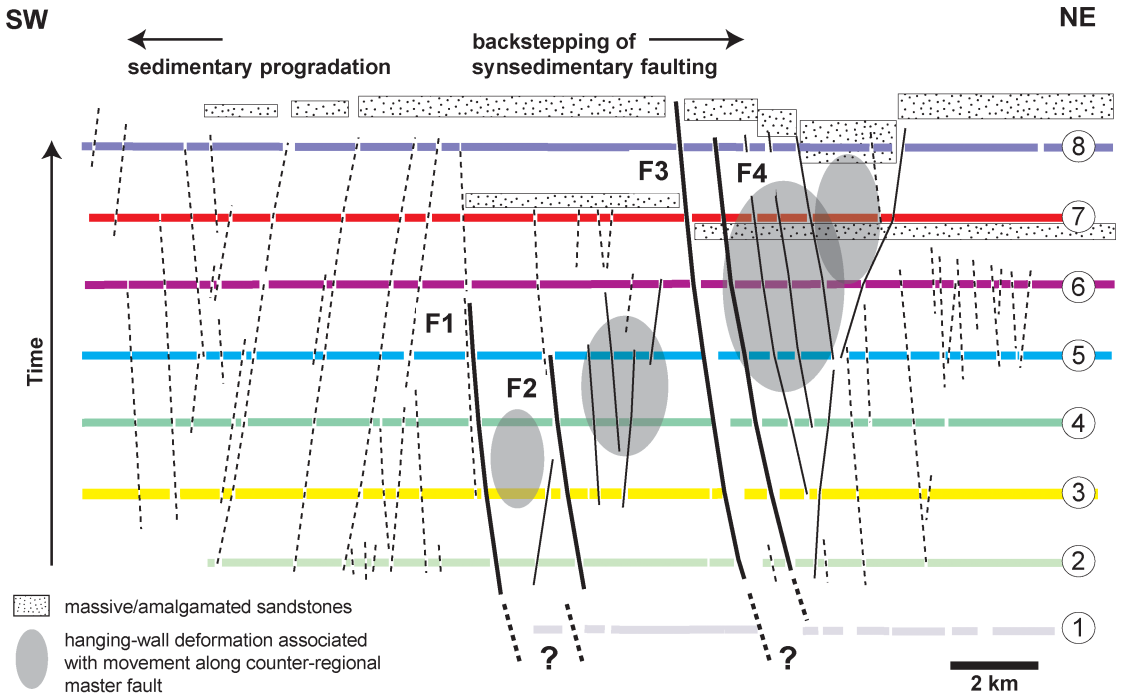
SW
NE
sedimentary progradation
backstepping of
synsedimentary faulting
F1
F2
F3
F4
Time
8
7
6
5
4
3
2
1
?
?
2 km
massive/amalgamated sandstones
hanging-wall deformation associated
with movement along counter-regional
master fault

Figure 7

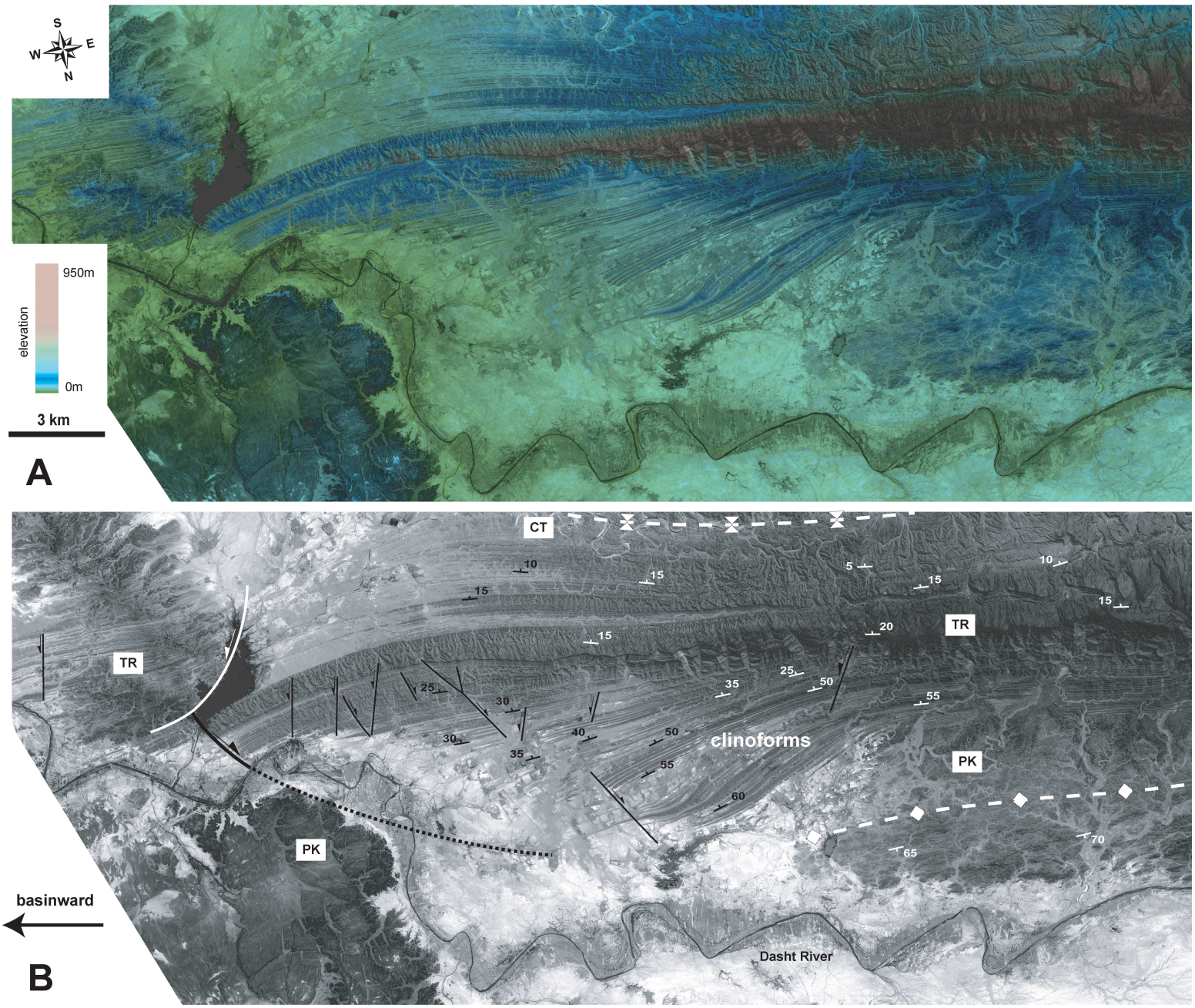
S
W
E
N
950m
elevation
0m
3 km
A
CT
TR
PK
clinoforms
basinward
B
Dasht River
main sediment transport direction
Fig. 10
C
massive/amalgamated sandstones
interbedded shales and sandstone
deformed, possibly slumped shales
mudstones

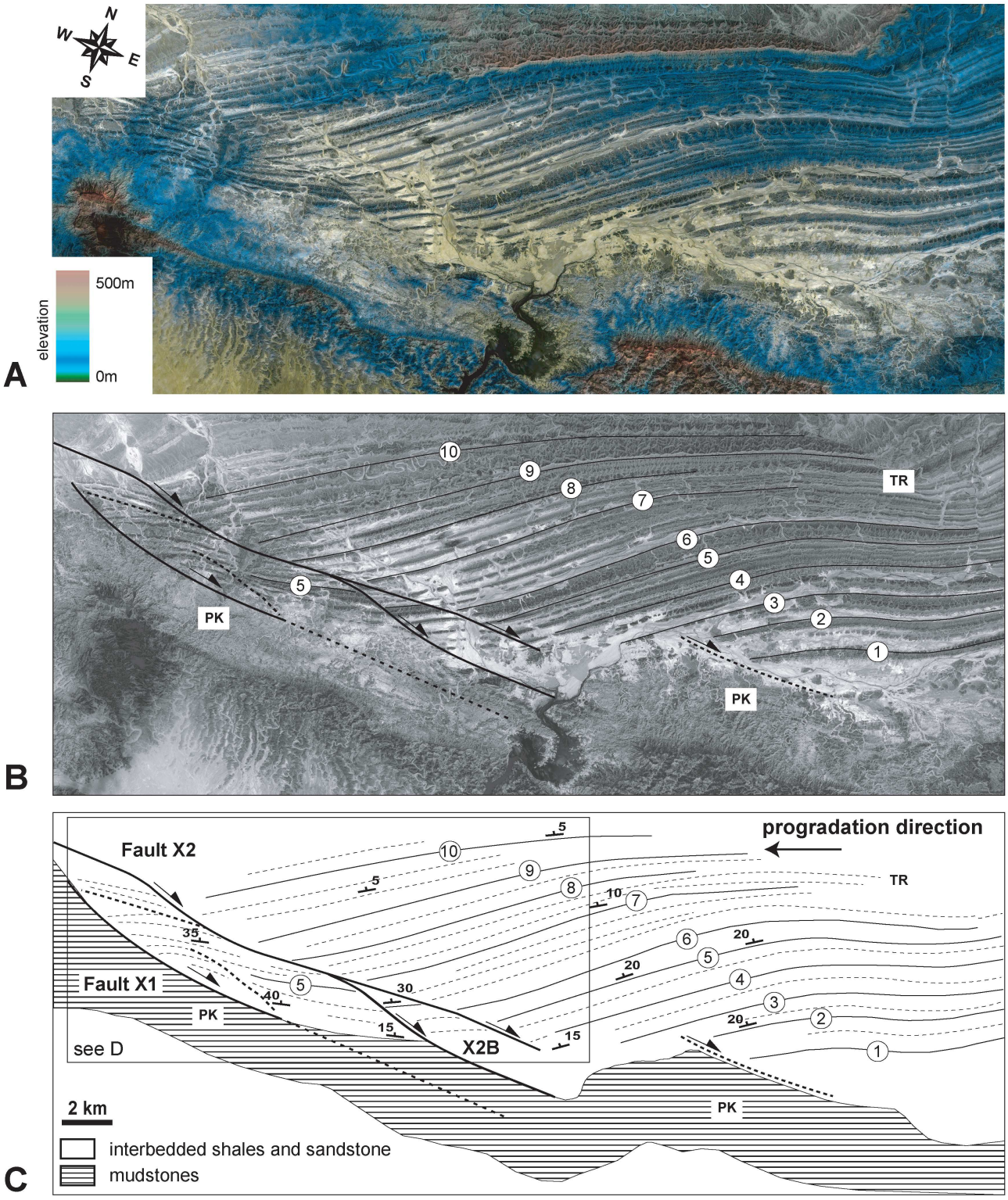
A
N
W
E
S
elevation
500m
0m
B
TR
PK
PK
C
Fault X2
progradation direction
TR
Fault X1
PK
see D
X2B
2 km
PK
interbedded shales and sandstone
mudstones
D
Fault X2
(U)
(M)
(L)
Fault X1
2 km
X2B
1 km

Figure 8

Figure 9

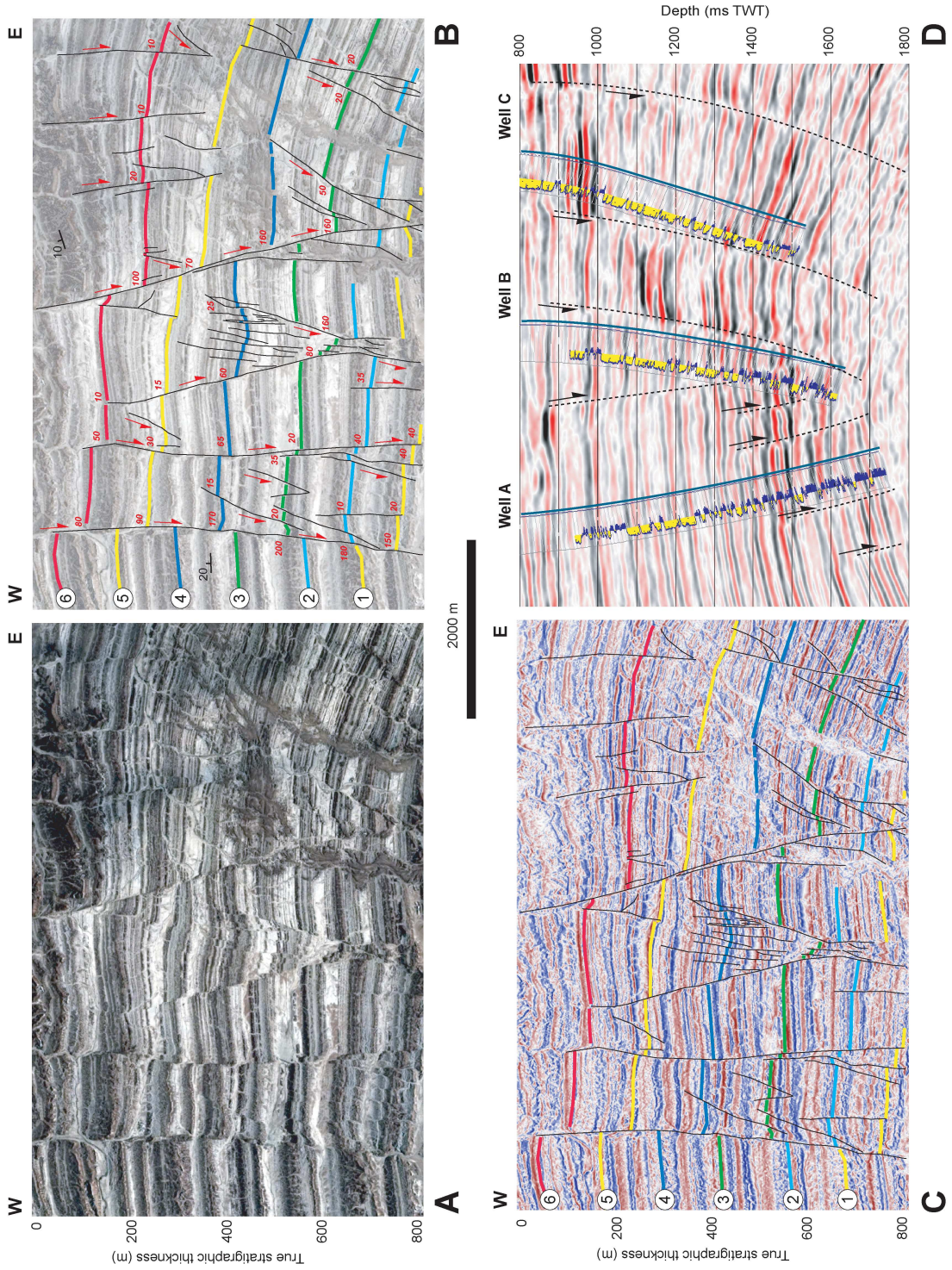
A
B
C
D
W
E
True stratigraphic thickness (m)
0
200
400
600
800
2000 m
Depth (ms TWT)
800
1000
1200
1400
1600
1800
Well A
Well B
Well C
1
2
3
4
5
6

Figure 10

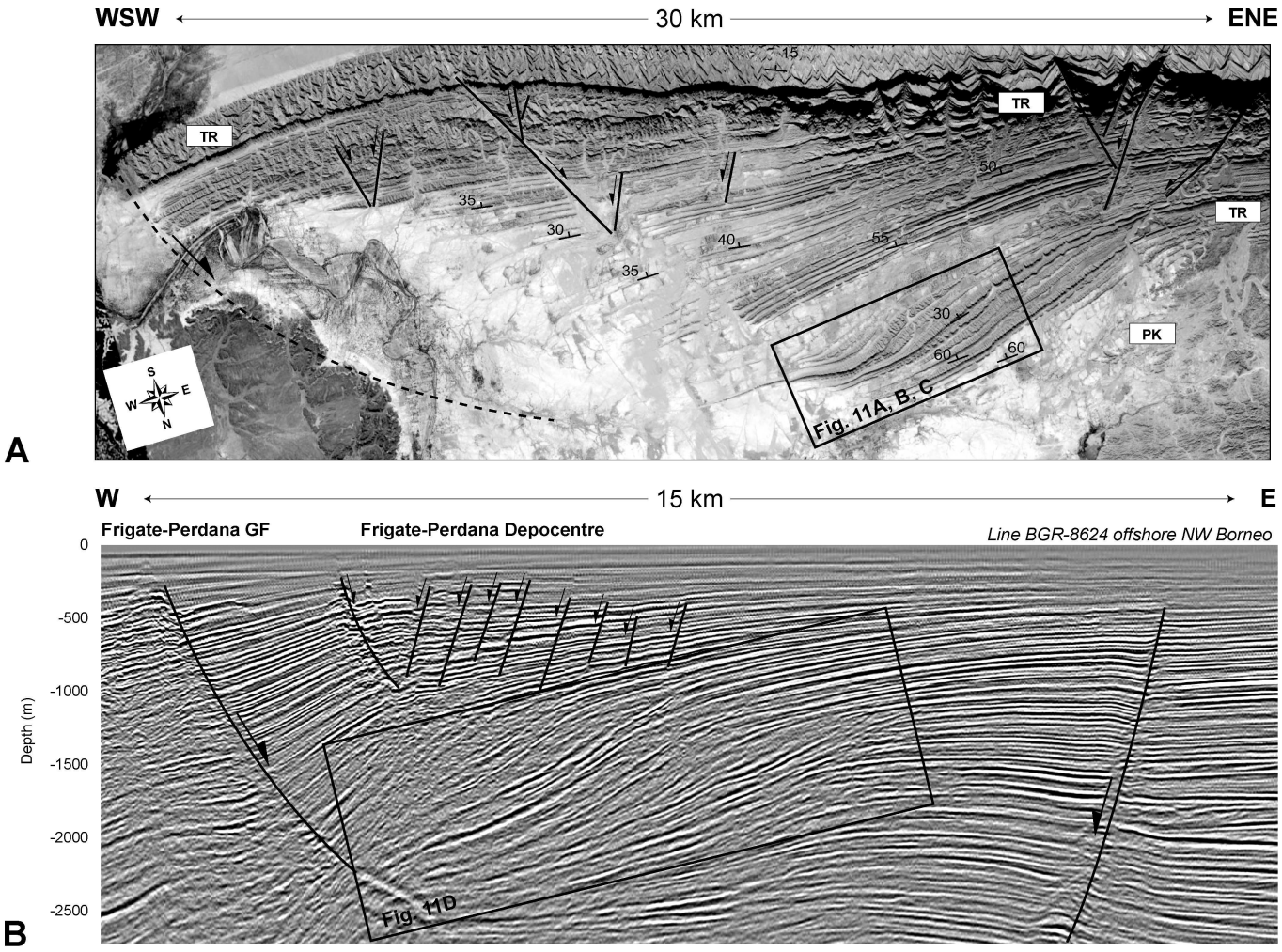
WSW
30 km
ENE
TR
TR
TR
PK
15
50
35
30
40
55
35
30
60
60
Fig. 11A, B, C
S
W
E
N
A
W
15 km
E
Frigate-Perdana GF
Frigate-Perdana Depocentre
Line BGR-8624 offshore NW Borneo
Depth (m)
0
-500
-1000
-1500
-2000
-2500
Fig. 11D
B

Figure 11

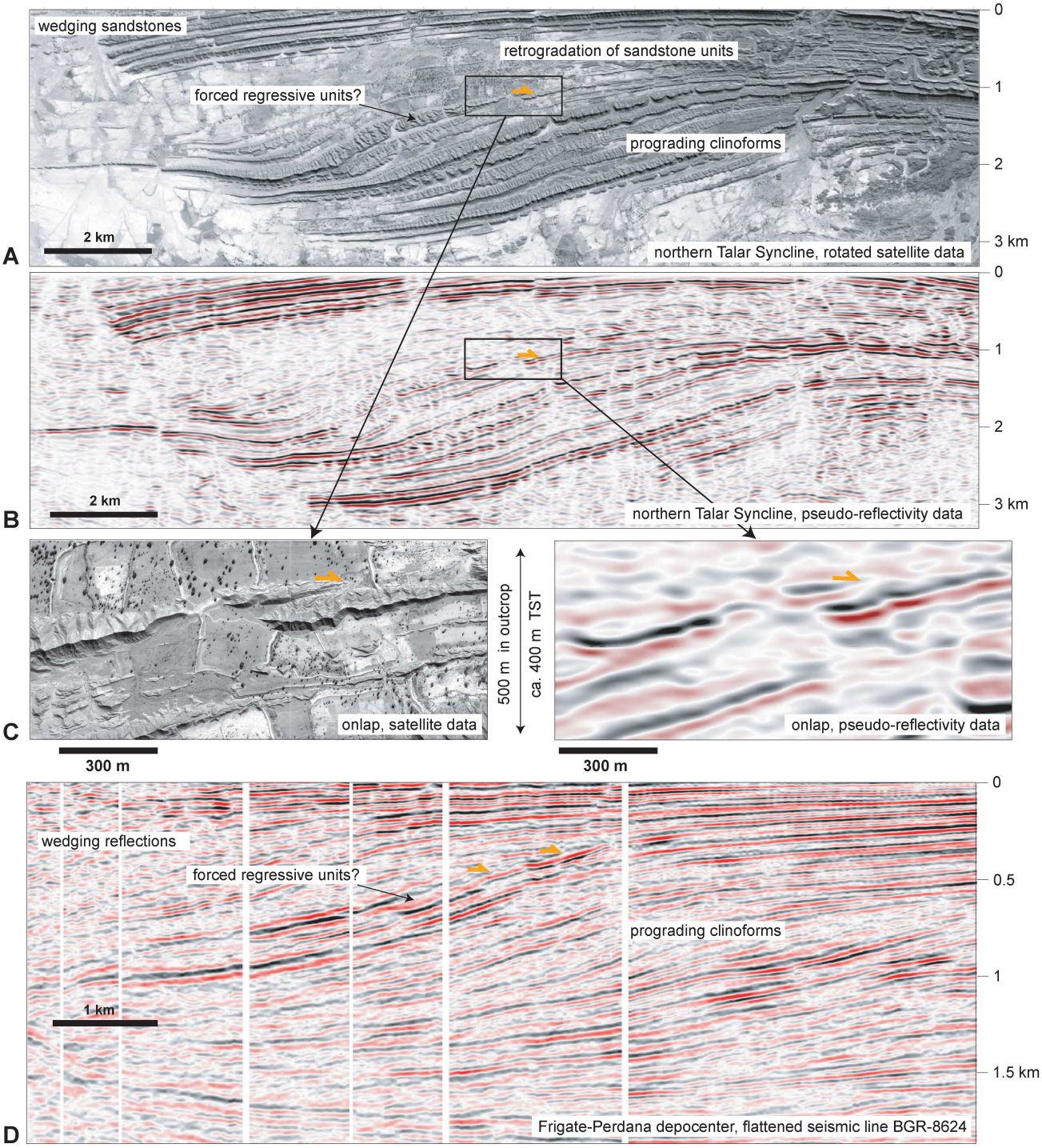
A
wedging sandstones
retrogradation of sandstone units
forced regressive units?
prograding clinoforms
2 km
northern Talar Syncline, rotated satellite data
0
1
2
3 km
B
2 km
northern Talar Syncline, pseudo-reflectivity data
0
1
2
3 km
C
onlap, satellite data
300 m
500 m in outcrop
ca. 400 m TST
onlap, pseudo-reflectivity data
300 m
D
wedging reflections
forced regressive units?
1 km
prograding clinoforms
Frigate-Perdana depocenter, flattened seismic line BGR-8624
0
0.5
1
1.5 km

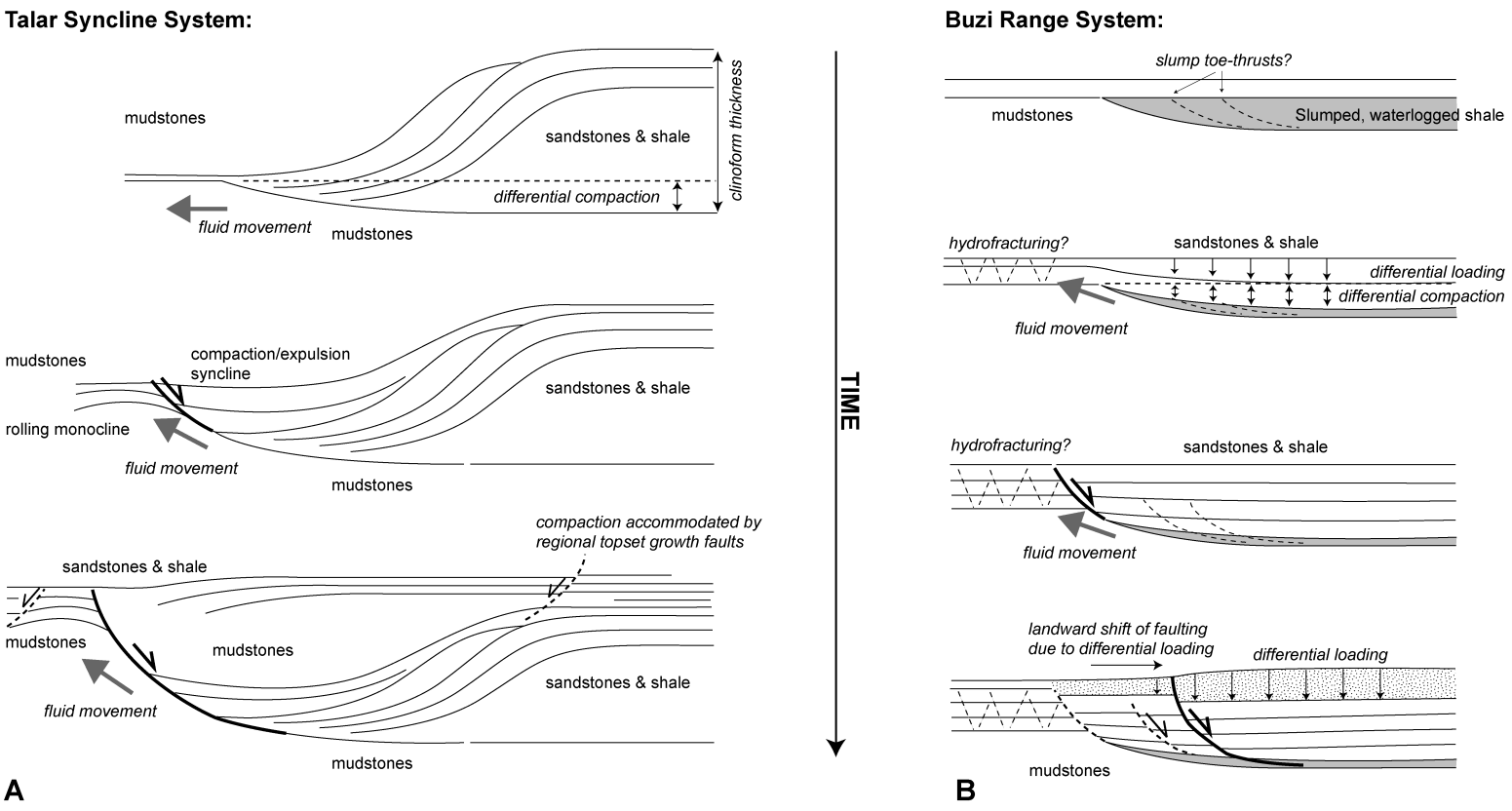
Talar Syncline System:
mudstones
sandstones & shale
clinoform thickness
differential compaction
fluid movement
mudstones
mudstones
compaction/expulsion syncline
sandstones & shale
rolling monocline
fluid movement
mudstones
compaction accommodated by regional topset growth faults
sandstones & shale
mudstones
mudstones
sandstones & shale
fluid movement
mudstones
A
TIME
Buzi Range System:
slump toe-thrusts?
mudstones
Slumped, waterlogged shale
hydrofracturing?
sandstones & shale
differential loading
differential compaction
fluid movement
hydrofracturing?
sandstones & shale
fluid movement
landward shift of faulting due to differential loading
differential loading
mudstones
B

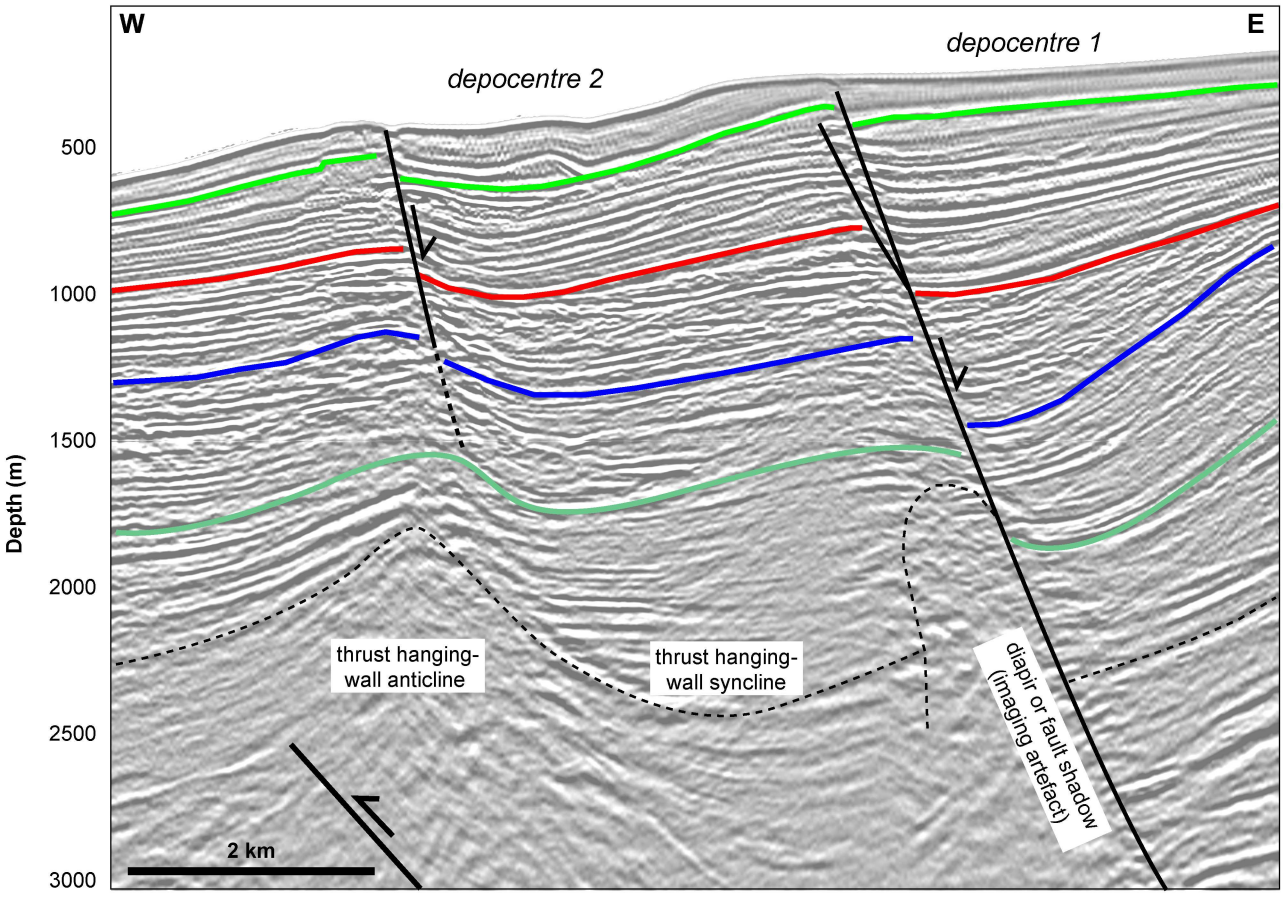

Line BGR-8624 offshore NW Borneo, upper slope